

CHARACTERIZATION OF THE IBR5-PAD1 INTERACTION IN ARABIDOPSIS
AUXIN RESPONSE

by

Nicholas C. Siepert, B.S.

A thesis submitted to the Graduate Council of
Texas State University in partial fulfillment
of the requirements for the degree of
Master of Science
with a Major in Biology
December 2017

Committee Members:

Nihal Dharmasiri, Chair

Sunethra Dharmasiri

Hong-Gu Kang

Dana García

COPYRIGHT

by

Nicholas C. Siepert

2017

FAIR USE AND AUTHOR'S PERMISSION STATEMENT

Fair Use

This work is protected by the Copyright Laws of the United States (Public Law 94-553, section 107). Consistent with fair use as defined in the Copyright Laws, brief quotations from this material are allowed with proper acknowledgment. Use of this material for financial gain without the author's express written permission is not allowed.

Duplication Permission

As the copyright holder of this work I, Nicholas C. Siefert, authorize duplication of this work, in whole or in part, for educational or scholarly purposes only.

ACKNOWLEDGEMENTS

My sincere thanks go to my research supervisor Dr. Nihal Dharmasiri and my thesis committee member Dr. Sunethra Dharmasiri for their advice and support throughout my graduate studies. My gratitude also goes to Dr. Kang and Dr. Garcia for their input and expertise. Thank you to Dr. Praveen Kumar and to Thilanka Jayaweera for their guidance and assistance in learning new techniques. I have to acknowledge former and present Dharmasiri lab members for their helpful insights and their friendly attitudes. Finally, I'd like to thank my family for encouraging me throughout this endeavor.

This research was made possible by National Science Foundation (NSF) grant IOS-0845305 to Dr. Nihal Dharmasiri. NSF grant DBI-0821252 to Dr. Dana Garcia & Dr. Joseph Koke. One time Texas State University grant REP-9000000525 to Drs. Nihal & Sunethra Dharmasiri.

TABLE OF CONTENTS

	Page
ACKNOWLEDGEMENTS	iv
LIST OF FIGURES	vi
ABSTRACT	viii
CHAPTER	
I. INTRODUCTION	1
II. MATERIALS AND METHODS.....	13
III. RESULTS	27
IV. DISCUSSION	49
REFERENCES	64

LIST OF FIGURES

Figure	Page
1. Endogenous and synthetic auxins contain similar structural features	2
2. The 26S proteasome is assembled from the 20S and 19S complexes	5
3. Auxin signaling.....	7
4. IBR5 interacts with PAD1 <i>in vitro</i>	28
5. The CBD of IBR5 is required for interaction with PAD1	29
6. The N-terminal portion of PAD1 is required for interaction with IBR5	31
7. IBR5 interacts with PAD1 <i>in vivo</i>	32
8. PAD1 and IBR5 co-localize to the cytosol and the nucleus	34
9. <i>pad1</i> and <i>pad2</i> T-DNA mutant lines are homozygous	37
10. Heterozygous <i>pad1/+ pad2/+</i> double mutants have fewer seeds within siliques	39
11. Heterozygous <i>pad1/+ pad2/+</i> plants produce significantly fewer viable pollen grains compared to WT or either single mutant.....	40
12. Primary roots of <i>pad1</i> and <i>ibr5-1</i> mutants are longer than WT roots when grown on 2,4-D	42
13. The <i>pad1 ibr5-1</i> double mutant is more resistant to primary root growth inhibition by 2,4-D than either of the <i>pad1</i> or <i>ibr5-1</i> single mutants	43
14. <i>pad1</i> , <i>ibr5-1</i> , and <i>pad1 ibr5-1</i> mutant lines are resistant to 70 nM IAA	44
15. The <i>pad2</i> T-DNA mutant line displays an auxin-resistant phenotype.....	45
16. Expression of PAD1-HA in <i>pad1</i> mutant background recovers the mutant phenotype.....	45
17. Auxin responsive gene expression is altered in <i>ibr5-1</i> , <i>pad1</i> , and <i>ibr5-1 pad1</i> mutants.....	47
18. <i>pad1</i> partially recovers the AXR3NT-GUS destabilization in <i>ibr5-4</i>	48
19. DII-Venus protein levels are slightly stabilized in <i>pad1</i>	48
20. Putative phospho-sites of the proteasomal $\alpha 4$ subunit and 3D representation of PAD1.....	54

21. Reversible phosphorylation of PAD1 may regulate 26S proteasome activity.....60

ABSTRACT

Many plant hormones utilize the ubiquitin-proteasome system (UPS) to modulate the expression of specific genes involved in various developmental processes as well as responses to environmental stress. In this process the target proteins are polyubiquitinated by a multi-subunit E3 ubiquitin ligase complex, essentially tagging the target proteins for degradation by the 26S proteasome. One specific type of E3 ligase, the SKP1-CULLIN1-F-BOX protein (SCF) complex, is utilized by several plant hormones to ubiquitinate target proteins. This process is highly specific and requires multiple levels of regulation which are not fully understood. Recent studies have shown that the *INDOLE-3-BUTYRIC ACID RESPONSE5 (IBR5)* gene, which encodes a dual specificity phosphatase, plays an important role in the auxin signaling pathway. Previous studies suggest that IBR5 negatively regulates Aux/IAA repressor protein degradation. This research identifies and characterizes a novel interaction between IBR5 and PAD1, a subunit of the 20S core of the proteasome. The interaction between IBR5 and PAD1 was confirmed *in vitro* and *in vivo*. Additionally, specific domains or regions of each protein were identified to be crucial for this interaction. Similar to *ibr5* mutants, *pad1* and *pad2* displayed auxin-resistant phenotypes. Furthermore, the *pad1* mutation partially rescued the AXR3NT-GUS destabilization in *ibr5-4*. Taken together, these findings suggest that the interaction between IBR5 and PAD1 may play a role in the regulation of auxin signaling and the UPS.

CHAPTER I

INTRODUCTION

Plant growth and development are highly regulated processes which are under hormonal and environmental control. Due to their sessile nature, plants have evolved mechanisms to respond quickly and appropriately to their environment, and these responses are coordinated by various hormones within the plant. Certain internal and external stimuli promote the synthesis of phytohormones or conversion into their active forms (Gray, 2004; Spiess et al., 2014; Wani et al., 2016). These phytohormones initiate signaling cascades, which can ultimately result in alterations of gene expression. One of the most important and extensively studied phytohormones is auxin, which is essential in a variety of developmental and physiological processes (Enders et al., 2015).

Indole-3-acetic acid (IAA) is the predominant endogenous auxin and is found in all plants (Lau et al., 2009). There are other endogenous auxins which produce similar effects in plants (Simon and Petrasek, 2011). One of these compounds, indole-3-butyric acid (IBA), functions as a precursor to IAA but may also act as an auxin on its own (Van Der Krieken, 1993; Zolman et al., 2000). There are many synthetic compounds that exhibit auxin-like activity; 2,4-D (2,4-dichlorophenoxyacetic acid) and picloram (4-amino-3,5,6-trichloropicolinic acid), for example, have been utilized in agriculture due to their auxin-like activity, in addition to being useful compounds for studying auxin signaling.

Endogenous and synthetic auxins have similar physiological effects, but their mechanisms of action may differ due to differences in their structures (Figure 1) (Simon et al., 2013).

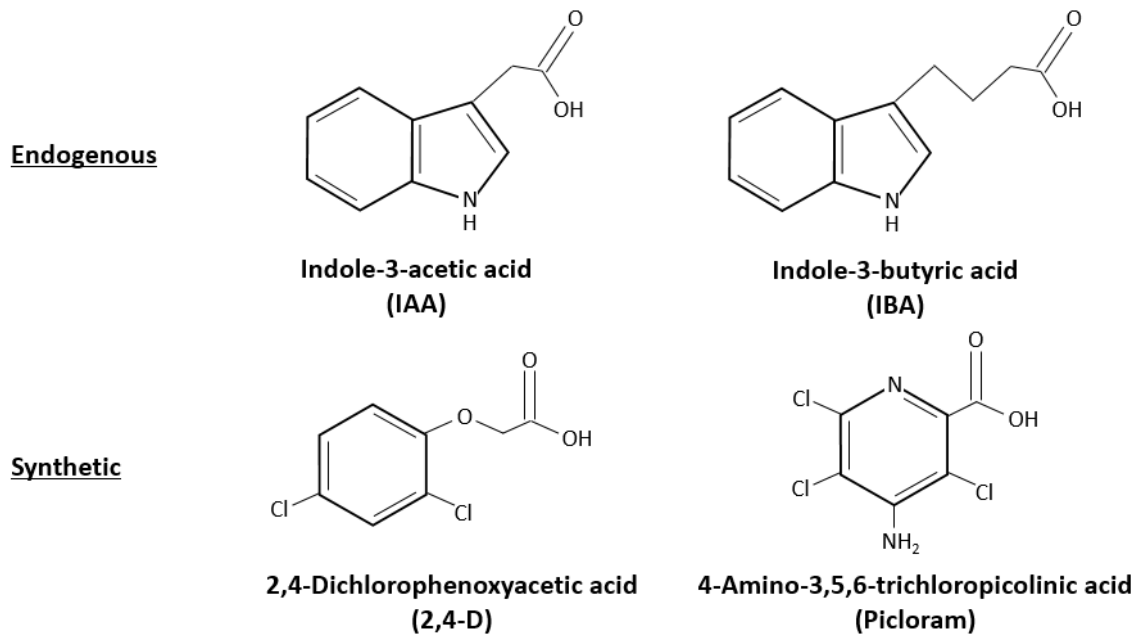


Figure 1. Endogenous and synthetic auxins contain similar structural features. The endogenous auxins indole-3-acetic acid (IAA) and indole-3-butyric acid (IBA) possess an aromatic ring and a carboxylic acid group, similar to the synthetic auxins 2,4-dichlorophenoxyacetic acid (2,4-D) and 4-amino-3,5,6-trichloropicolinic acid (picloram).

Auxin gradients within root and shoot tissues are essential for proper development throughout the life of the plant (Overvoorde et al., 2010; Gallavotti et al., 2013). Auxin is also responsible for cell expansion, as described in the long-standing “acid growth theory,” by which auxin promotes the loosening and expansion of cell walls in order to facilitate cell elongation (Rayle et al., 1992). Auxin responses involve a group of transcription factors known as auxin response factors (ARFs), which modulate the expression of auxin responsive genes by binding to the auxin response elements (AuxREs) in their regulatory regions (Guilfoyle et al., 2007). A set of repressors known as Aux/IAA proteins bind ARFs

and suppress their activity (Guilfoyle et al., 2007). Auxin promotes the degradation of Aux/IAA repressor proteins, thus relieving ARF repression and allowing modulation of auxin response gene expression (Gray et al., 2001).

The study of auxin signaling mutants often requires the analysis of primary auxin response genes, which are typically members of the *Aux/IAA*, *GH3*, or *SAUR* gene families (Abel & Theologis, 1996). In *Arabidopsis* there are 29 *Aux/IAA* genes, which encode short-lived repressor proteins that suppress ARF activity. Most of the Aux/IAA proteins carry four distinct domains. Domain I has been shown to interact with the transcriptional co-repressor protein TPL (TOPELESS) (Szemenyei et al., 2008). Domain II possesses a degron motif, which contains a thirteen amino acid long sequence that is essential for degradation of these proteins (Hagen & Guilfoyle, 2002, Villalobos et al., 2012). Domains III and IV facilitate heterodimerization with other Aux/IAA proteins and with ARF proteins (Kim et al., 1997; Tiwari et al., 2004).

The *GH3* gene family contains 19 genes, which encode proteins that function in IAA-amido synthesis (Fu et al., 2011). By controlling free IAA levels, GH3 proteins contribute to the regulation of tropic responses, apical dominance, and IAA metabolism (Rogg et al., 2001; Uehara et al., 2008; Nagpal et al., 2000; Staswick et al., 2005). The *SAUR* (*Small Auxin Upregulated RNA*) gene family contains over 72 genes, which encode generally unstable proteins or mRNA transcripts with destabilizing motifs (Gil and Green, 1996; Knauss et al., 2003). These destabilizing motifs bind to heterologous transcripts, resulting in rapid reduction of heterologous transcript levels (Newman et al., 1993). More recently, SAUR19 was shown to inhibit PP2C.D phosphatases, resulting in increased cell expansion (Ren & Gray, 2015). Several SAUR proteins have also been shown to play a

role in ethylene signaling, suggesting that the SAUR gene family may be important for phytohormone crosstalk (Li et al., 2015).

Auxin promotes the degradation of Aux/IAA repressor proteins through the ubiquitin-proteasome system (UPS), a mechanism for targeted protein degradation that is utilized by all eukaryotes. The ability of this system to rapidly degrade regulatory proteins makes it an essential component of many signaling pathways. The UPS in plants is involved in a variety of processes, including hormone signaling, tissue differentiation, chromatin structure, and responses to the environment (Tomko et al., 2013; Vierstra et al., 2009). Two protein complexes of interest within the UPS include the 26S proteasome and the E3 ubiquitin ligase. The 26S proteasome is a large protein complex with compartmentalized proteolytic activity. This complex consists of a 20S core particle (CP) and a 19S regulatory particle (RP). The 20S complex is composed of four heptameric rings; two inner rings composed of β -subunits, and two outer rings composed of α -subunits. The β -subunits confer trypsin-like, chymotrypsin-like, and caspase-like peptidase activity to the hollow interior of the 20S CP, while the α -subunits facilitate interaction with the 19S RP (Baumeister et al., 1998; Bedford et al., 2010). The 19S RP is made up of a base portion and a lid portion. The base of the 19S RP features AAA-ATPases (ATPases associated with diverse cellular activities), which convert energy from ATP into mechanical energy that is used to unfold proteins and shuttle them into the proteasome for degradation (Yedidi et al., 2017). The lid of the 19S RP consists of ubiquitin (UBQ) recognition sites for recruitment of polyubiquitinated proteins, as well as a metalloprotease for deubiquitination of said proteins (Figure 2) (Baumeister et al., 1998; Förster et al., 2014).

Auxin promotes the degradation of Aux/IAA repressor proteins by promoting their ubiquitination (see Dharmasiri et al., 2013 for review). Ubiquitin is covalently attached to target proteins via E3 ubiquitin ligases, allowing the target proteins to be recognized by the 26S proteasome for degradation (Choi et al., 2014). Ubiquitination of target proteins begins

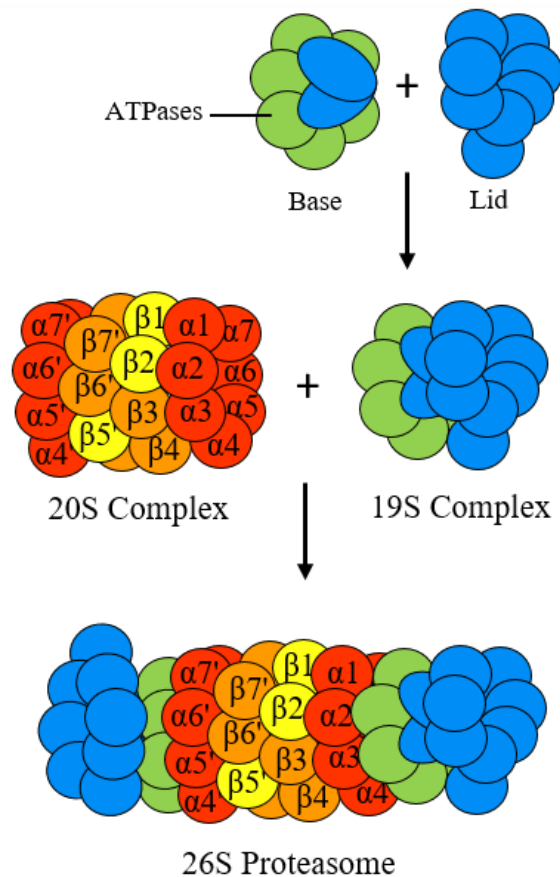


Figure 2. The 26S proteasome is assembled from the 20S and 19S complexes. The 19S regulatory complex is comprised of a lid and base region containing ATPases. The 20S core complex consists of two heptameric inner rings composed of β -subunits, and two heptameric outer rings composed of α -subunits.

with the activation of UBQ by the E1 UBQ activating enzyme, followed by conjugation to the E2 enzyme. The UBQ-conjugating E2 enzyme then binds to RBX1 (RING BOX-1), and the UBQ protein is transferred to a lysine residue of the target protein presented by the

SCF complex. The SCF E3 ubiquitin ligase consists of several core components; CUL1 (Cullin1), Skp1 (S-PHASE KINASE-ASSOCIATED PROTEIN 1), RBX1, and an F-box protein. CUL1 acts as a scaffold, connecting RBX1 and the E2 UBQ-conjugating enzyme to specific substrate adaptors such as ASK1 (ARABIDOPSIS SKIP) and an F-box protein such as TIR1 (TRANSPORT INHIBITOR RESPONSE 1) in the case of auxin-mediated protein degradation (Choi et al., 2014). There are F-box proteins in plants that function in a variety of hormonal signaling pathways, including COI1 in jasmonate signaling, SLY1 in gibberellic acid signaling, EBF1/EBF2 in ethylene signaling, and TIR1/AFBs proteins in auxin signaling (Dharmasiri et al., 2013). All of these F-box proteins, and more, use ASK1 as an adapter to interact with Cullin/RBX1 based E3 ubiquitin ligases (CRLs) (Willems et al., 2004; Dharmasiri et al., 2013; Choi et al., 2014). TIR1/AFBs proteins typically have a large leucine-rich repeat domain responsible for target protein specificity (Yu et al., 2015). Auxin acts as a “molecular glue” to increase the affinity between the F-box protein, TIR1, and Aux/IAA repressor proteins, resulting in the polyubiquitination and subsequent degradation of the Aux/IAA repressor proteins (Figure 3) (Dharmasiri et al., 2005; Tan et al., 2007).

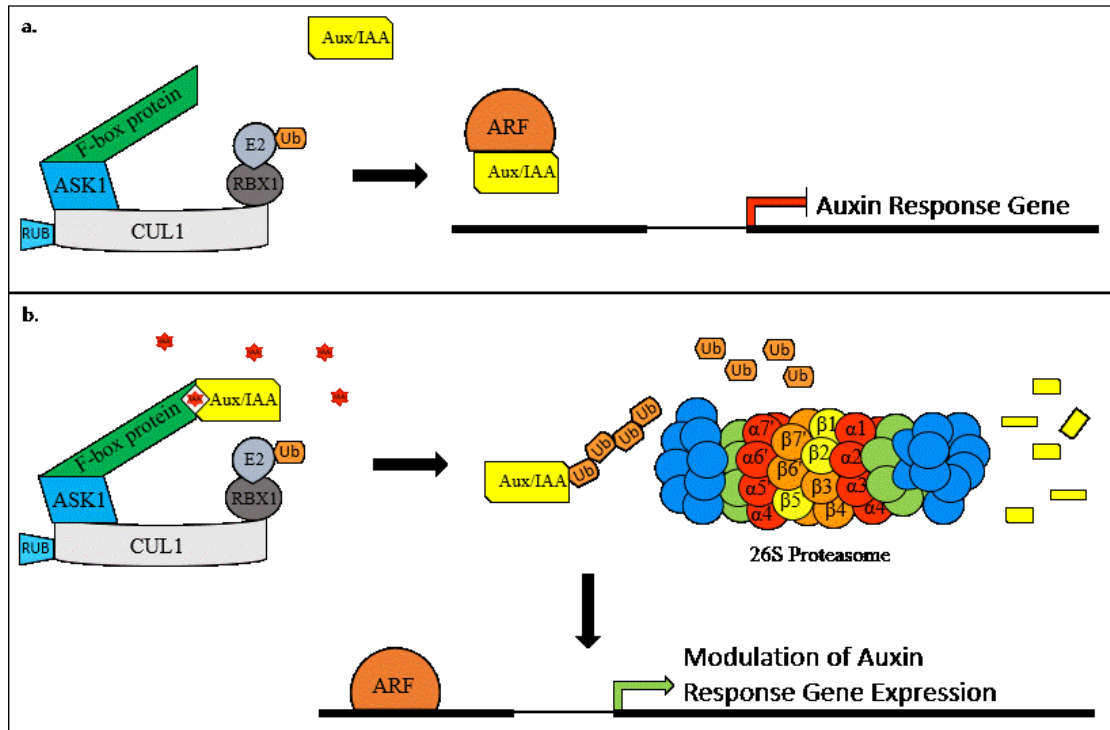


Figure 3. Auxin signaling. (a) Auxin responsive genes are repressed under low auxin conditions by Aux/IAA repressor proteins. (b) Increased auxin levels promote the polyubiquitination and subsequent degradation of Aux/IAA repressor proteins through the 26S proteasome, allowing for ARFs to modulate auxin responsive gene expression.

SCF E3 ubiquitin ligase mediated protein degradation can be precisely modulated, due to high levels of specificity and regulation (Abel et al., 1994; Dharmasiri et al., 2005). The SCF complex is constantly recruiting target proteins, facilitated by ASK1 and F-box proteins. Additionally, the E3 ligase is constantly cycling through an active and inactive state (Willems et al., 2004, Choi et al., 2014). RUB1 (related-to-ubiquitin) is conjugated to CUL1 by the enzyme RCE1 (RUB-conjugating enzyme), in effect, activating the SCF^{TIR1} E3 ligase (Dharmasiri et al., 2003). In this active state, ASK1 and TIR1 can freely interact with CUL1, and polyubiquitination of Aux/IAA proteins can occur. ASK1 and TIR1 must be dissociated from the CUL1-RBX1 complex before new target proteins can be recruited. Dissociation is accomplished by the CSN (COP9/signalosome), which cleaves the RUB1

modification from CUL1. Interestingly, the CSN complex resembles the lid of the 26S proteasome's 19S regulatory complex. The protein CAND1 (cullin-associated and neddylation/rubylation-dissociated) is able to interact with the unmodified CUL1-RBX1 complex and prevents ASK1-F-box protein complexes from interacting with CUL1. Conjugation of a new RUB1 protein results in dissociation of CAND1 (Willems et al., 2004). This process creates an equilibrium between active and inactive complexes that also allows for the recruitment of new target proteins. It is also interesting to note that the CSN and CAND1 were found to interact with the ATPases in the base portion of the proteasomal 19S complex (Huang et al., 2005; Makino et al., 1999;).

Recent studies have shown that the *INDOLE-3-BUTYRIC ACID RESPONSE5* (*IBR5*) gene encodes a dual specificity phosphatase that regulates auxin responses (Strader et al., 2008; Jayaweera et al., 2014). Dual specificity phosphatases can dephosphorylate serine, threonine, and tyrosine residues of their substrates (Gupta et al., 1998). These types of phosphatases are involved in various signaling process, such as phytohormone responses and environmental stress responses (Bartels et al., 2010). *IBR5* was shown to interact with and dephosphorylate the mitogen-activated protein kinase MPK12, an important regulator of stress and hormonal responses in plants (Lee et al., 2009). More recently, *IBR5* was shown to interact with the stress response chaperone proteins HSP90 (heat shock protein 90) and SGT1b (suppressor of G2 allele of SKP1 homolog B) and act as a holdase to stabilize CHS3 (chilling sensitive 3) proteins (Liu et al., 2015). Mutations in *IBR5* result in various developmental defects, including stunted growth, reduced leaves, and insensitivity to auxin. Overexpression of a catalytically inactive version of *IBR5* in the knockout mutant background was able to partially recover some of the mutant phenotypes

(Strader et al., 2008). Taken together, these results suggest that IBR5 has multiple functions in hormone and stress responses, some of which may be independent of its phosphatase activity.

It was revealed that IBR5 interacts with the SCF complex component ASK1, using high-throughput binary interactome mapping (a modified yeast two-hybrid system) (Braun et al., 2011). This interaction was confirmed *in vivo* by co-immunoprecipitating ASK1 with IBR5-Myc (Jayaweera, unpublished). This interaction represents a physical connection between IBR5 and the auxin signaling pathway, as well as other hormone signaling pathways that utilize ASK1, such as gibberellic acid, jasmonate, and ethylene responses (Dharmasiri et al., 2013).

An important component of developmental and environmental signal transduction in plants is the secondary messenger Ca^{2+} (Kudla et al., 2010; Hepler et al., 1985; Bush, 1995). Regulatory proteins known as calmodulins (CaMs) change their conformation upon binding Ca^{2+} ions. These changes allow CaMs to interact with and modulate the function of various proteins, including kinases, phosphatases, and other metabolic enzymes (Perochon et al., 2011; Bouché et al., 2005). Ca^{2+} /CaM has been linked to auxin signaling through interactions with SAUR proteins and the IAA31 repressor protein (Yang and Poovaiah, 2000; Popescu et al., 2007). Additionally, a study in rice shows that Ca^{2+} /CaM plays an important role in IBA-induced formation of lateral roots (Chen & Kao, 2012). Recent findings from our lab suggest that Ca^{2+} stabilizes Aux/IAA repressor proteins and that IBR5 interacts with CaM1 and CaM3 in a Ca^{2+} -dependent manner. IBR5 has a calmodulin-binding domain (CBD) that interacts with CaM, and which also overlaps with IBR5's catalytic domain (Jayaweera et al., unpublished). These results suggest that

Ca²⁺/CaM may have a role in auxin signaling that functions through interaction and modulation of IBR5.

The *ibr5-1* mutant, a null mutation in the *IBR5* gene, was identified through a mutant screen for primary root growth resistance to exogenous indole-3-butyric acid (IBA), a natural precursor to the auxin indole-3-acetic acid (IAA) (Enders et al., 2015; Page et al., 2002; Monroe-Augustus et al., 2003). Our lab identified *ibr5-4*, another *IBR5* mutant allele through a screen of ethyl methanesulfonate generated mutants for resistance to the synthetic auxin picloram. This mutant allele has a point mutation that results in substitution of Gly¹³² with Glu in the catalytic site of IBR5 (Jayaweera et al., 2014). Additionally, *IBR5* mRNA undergoes alternative splicing, producing IBR5.1 and IBR5.3 isoforms. IBR5.1 possesses phosphatase activity and is localized to the cytosol and nucleus, while IBR5.3 does not have phosphatase activity and is localized exclusively to the nucleus, suggesting that *IBR5* may have multiple functions (Jayaweera et al., 2014). *IBR5* mutant alleles and overexpression lines were analyzed in order to elucidate the functions of *IBR5* with respect to auxin signaling (Strader et al., 2008; Jayaweera et al., 2014; Monroe-Augustus et al., 2003). It has been shown that *ibr5-1* enhances many of the phenotypes of the F-box protein mutant *tir1*, including increased resistance to exogenous auxin such as IBA and the synthetic auxin 2,4-D (Strader et al., 2008).

Aux/IAA repressor proteins are degraded in the presence of auxin, resulting in an increase in auxin-inducible gene expression (Shimizu-Mitao et al., 2014; Rogg et al., 2001; Ulmasov et al., 1997; Hagen & Guilfoyle, 2002). Like many auxin response mutants, *ibr5-1* and *ibr5-4* experience a downregulation of auxin response genes (Strader et al., 2008; Jayaweera et al., 2014). qRT-PCR analysis revealed that *ibr5-4* has significantly less *IAA12*

and *IAA28* transcripts as compared with the wild type plants (WT) (Jayaweera et al., 2014). Surprisingly, Aux/IAA repressor proteins are destabilized in *ibr5* mutants (Strader et al., 2008; Jayaweera et al., 2014).

HS::AXR3NT-GUS, which contains Aux/IAA protein domains I and II, is a commonly used reporter gene construct for assessing the stability of Aux/IAA repressor proteins (Gray et al., 2001). Expression of this construct is induced by heat shock and can easily be detected by GUS histochemical assay (Gray et al., 2001). A mutant version of this reporter gene construct, *HS::axr3-INT-GUS*, was also developed in which *axr3-INT-GUS* proteins have low affinity for SCF^{TIR1}, resulting in increased stability of the reporter construct (Gray et al., 2001). AXR3NT-GUS is greatly reduced in the *ibr5-1* mutant background as compared with WT, whereas *axr3-INT-GUS* levels are relatively equal in *ibr5-1* and WT root tips (Strader et al., 2008). Reduced AXR3NT-GUS levels can also be observed in the *ibr5-4* mutant (Jayaweera et al., 2014). Additionally, AXR3NT-GUS can be stabilized in *ibr5-1* upon treatment with the 26S proteasome inhibitor MG132 (Strader et al., 2008). These findings show that Aux/IAA repressor proteins are destabilized in the *ibr5-1* and *ibr5-4* mutants, and suggest that depletion of these proteins may be at least partially facilitated by the 26S proteasome and SCF^{TIR1}-mediated protein degradation.

In an attempt to elucidate the role of IBR5 in auxin signaling, our lab identified several IBR5-interacting proteins using yeast two-hybrid screening (P. Kathare, unpublished). One of the IBR5 interacting proteins, PAD1, is an $\alpha 4$ subunit of the 20S core of the proteasome. PAD1 and its homolog PAD2 have 95% identical amino acid sequences (Fu et al., 1998). Both PAD1 and PAD2 possess a lysine (K) and glutamate (E)-rich region towards their C-terminal ends, termed a “KEKE” motif, which extends outward from the

proteasome complex (Realini et al., 1994). This “KEKE” motif is present in five of the seven 20S proteasome α -subunits in Arabidopsis, and may play a role in mediating interactions with the 19S regulatory particle and other regulatory complexes (Whitby et al., 2000; Realini et al., 1994). Previous studies suggest that the “KEKE” motif may be involved in an interaction between PAD1 and the SKP1 adaptor component (ASK1 in Arabidopsis) of the SCF complex, as well as the SnRK1 (sucrose non-fermenting related kinase) isoforms AKIN10 and AKIN11 (Realini et al., 1994; Farrás et al., 2001; Arnim et al., 2001). Considering the established connections between IBR5, the SCF complex, and the 26S proteasome, we selected PAD1 as a candidate protein for investigation, hypothesizing that an interaction between PAD1 and IBR5 plays a role in auxin signaling.

CHAPTER II

MATERIALS AND METHODS

Utilized genotypes and growth conditions

This study used *Arabidopsis thaliana* ecotype *Columbia* (WT) as the wild type, obtained from the Arabidopsis Biological Resource Center (ABRC). The mutant and transgenic lines used were in the Col-0 WT background. Mutant and transgenic lines used in this study were obtained as follows, *ibr5-1* from Dr. Bonnie Bartel, T-DNA mutants *pad1* (SALK_047984) and *pad2* (SALK_042314C) from ABRC, *35S::DII-Venus* from Dr. Teva Vernoux, and *HS::AXR3NT-GUS* from Dr. William Gray. *35S::DII-Venus ibr5-4* and *HS::AXR3NT-GUS ibr5-4* lines were generated by Thilanka Jayaweera. *35S::IBR5-Myc*, *35S::IBR5-GFP*, and *35S::PAD1-GFP* were constructed by Thilanka Jayaweera. *35S::DII-Venus pad1*, *35S::DII-Venus pad1 ibr5-4*, *HS::AXR3NT-GUS pad1*, *HS::AXR3NT-GUS pad1 ibr5-4*, and *pad1 ibr5-1* were all generated by crossing respective lines with *pad1* and selecting for homozygous lines. Heterozygous *pad1/+ pad2/+* double mutant plants were generated by crossing *pad1* with *pad2*. The *pad1* mutant line was backcrossed twice with the WT before crossing into the previously mentioned lines.

Seeds were surface sterilized with 40% commercial bleach/0.1% Triton X-100 solution and rinsed thoroughly with sterile DI water. Sterilized seeds were vernalized at 4°C for at least 24 hours before plating on *Arabidopsis thaliana* medium with 0.5% sucrose (ATS), pH 5.6 (Lincoln et al., 1990). Seedlings were grown in a growth chamber at 22°C

with continuous illumination (Dharmasiri et al., 2003). When necessary, potted plants were maintained at 21-22°C in a growth room with constant light.

Vector construction

To generate *35S::HA-PADI* construct for transient expression, the *PADI* coding region was amplified from WT cDNA using Phusion High-Fidelity DNA Polymerase (New England BioLabs) and PADI pENTR F and PADI Sall R primers (Table 1). Amplified fragments were directionally cloned into pENTR/D-TOPO vector (Invitrogen) according to manufacturer's instructions. Plasmids were then transformed into TOP10 *E. coli* cells and subsequently isolated for cloning into the pGWB15 destination vector using a Gateway LR Clonase (Invitrogen) reaction per manufacturer instructions. Plasmids were transformed into TOP10 *E. coli* cells and then subsequently isolated for transformation into the *Agrobacterium tumefaciens* strain GV3101 via electroporation.

PADI::PADI-HA was generated by amplifying the entire *PADI* gene along with 2000 base pairs upstream of the gene's start codon using pPADI pENTR F and PADI pENTR R primers (Table 1). The amplicon was cloned into pGWB13, and then into the *Agrobacterium tumefaciens* strain GV3101. *Agrobacterium* was grown for two days in liquid LB containing gentamycin (25 µg/ml), rifampicin (10 µg/ml), hygromycin B (50 µg/ml), and kanamycin A (50 µg/ml). Cells were pelleted and resuspended in inoculation media (5% sucrose & 0.02% Silwet-L77) before performing a floral dip vacuum infiltration of *pad1* plants (as described in Clough & Bent, 1998).

IBR5-Myc deletion constructs (D1, D2, ND1, D4, D6, NT, F-box, and D3) and GST-PAD1 (generated by Thilanka Jayaweera) were expressed in *E. coli* BL21 strain. To generate GST-PAD1 deletion constructs, PAD1 coding sequences were amplified from cDNA via Phusion High-Fidelity DNA Polymerase (New England BioLabs) using PAD1 BamHI F and PAD1 D1 R (for PAD1 D1), PAD1 D3 F and PAD1 D3 R (for PAD1 D2), and PAD1 D5 F and PAD1 SalI R (for PAD1 D3). These coding sequences were then ligated into the *EcoRV* site of pBluescript II SK (Stratagene). The plasmid vectors were transformed into TOP10 *E. coli*, isolated, and digested with *Bam*HI and *Sal*I. Digested inserts were then ligated into the *Bam*HI/*Sal*I site of pGEX-4T-3 (Pharmacia) expression vector, which was subsequently transformed into BL21 *E. coli* cells.

Recombinant protein expression in *E. coli*

To express recombinant proteins in *E. coli*, respective bacterial colonies or glycerol stocks were inoculated into liquid LB medium containing 100 µg/ml of carbenicillin and grown overnight in a shaker at 37°C. Overnight cultures were inoculated into a larger volume (100-200 ml) of LB with 100 µg/ml of carbenicillin and grown for an additional 2-3 hours in a shaker at 37°C. Once the optical densities of the cultures were between 0.6 and 0.8, IPTG (Gold Biotechnology) was added to a final concentration of 1 mM and the culture was incubated for 4-5 hours in a shaker at 30°C. Bacterial cells were then pelleted via centrifugation at 8,000 x g for 10 minutes and stored at -80°C until further use.

Bacterial pellets were re-suspended in PBS (phosphate buffered saline; 137 mM NaCl, 2.7 mM KCl, 10 mM NaH₂PO₄, 2 mM KH₂PO₄, pH 7.4), and cells were lysed via

sonication (3 times for 10-15 seconds, with 15-20 seconds on ice between sonications). PMSF (phenylmethylsulfonyl fluoride; Amresco) and Tween-20 (Sigma) were added to the crude cell lysates to final concentrations of 1 mM and 0.1%, respectively. Lysates were incubated on a rocker for 10 minutes at 4°C, and then immediately centrifuged at 10,000 x g for 10 minutes at 4°C. Supernatant was collected and incubated with glutathione-agarose beads (Sigma) for 2-18 hours on a rocker at 4°C to purify GST fusion proteins. Glutathione-agarose beads were then washed 3 times with PBS containing 0.1% Tween-20, and all washing buffer was removed after the final wash using a narrow pipette tip. Finally, the beads were re-suspended in PBS and stored at 4°C until ready for use. Bacterially expressed IBR5-Myc truncated proteins were stored as whole cell extracts (with 10% glycerol) at -80°C until ready for use.

***In vitro* pull-down assays**

Total protein was extracted from 8 day-old *35S::IBR5-Myc* seedlings using native protein extraction buffer comprising 50mM Tris-Cl, pH 7.5, 100 mM KCl, 10% glycerol, 0.1% Tween-20, 10 µM MG132 (26S proteasome inhibitor), 1 mM PMSF, and protease inhibitor cocktail from Roche. Crude extract was incubated on a rocker at 4°C for 10 minutes and then centrifuged at 10,000 x g for 10 minutes at 4°C. Supernatant was collected and stored at -80°C until ready for use.

35S::IBR5-Myc plant extract (approximately 800 to 1000 µg) was incubated with full-length GST-PAD1 or truncated GST-PAD1 proteins conjugated to glutathione-agarose beads for 3 hours on a rocker at 4°C. Beads were pelleted by brief centrifugation and

washed 4 times for 10 minutes each with 500 μ l of pull-down washing buffer (50 mM Tris-Cl, pH 7.5, 100 mM KCl, 10% glycerol, 0.1% Tween-20). Washing buffer was completely removed after the final wash with a narrow pipette tip, and the glutathione-agarose beads were re-suspended in 15 μ l of 2X Laemmli sample buffer (250 mM Tris-HCl, pH 6.8, 40 g/L SDS, 20% glycerol, 30 g/L bromophenol blue, 10% β -mercaptoethanol) and boiled for 6 minutes in preparation for SDS-PAGE and western blot analysis.

Pull-downs with EGTA were performed as described above with the addition of 4 mM EGTA to the incubation step and washing steps of the pull-downs. Pull-downs with bacterially expressed truncated IBR5-Myc proteins were performed as described above with the only substitution being PBS containing 0.1% Tween-20 in place of the pull-down washing buffer. All pull-down assays were performed a minimum of three times with similar results.

Transient protein expression

Agrobacterium tumefaciens strain GV3101 containing *35S::HA-PADI* was cultured in liquid LB medium with gentamycin (25 μ g/ml), rifampicin (10 μ g/ml), and hygromycin B (50 μ g/ml) for 2 days in a 30°C shaker. Bacterial cells were pelleted by centrifugation at 6,000 x g for 10 minutes and then re-suspended in a 5% sucrose solution to an optical density of 0.8. Roughly 10 ml of *Agrobacterium* solution was poured over 4 day old *35S::IBR5-Myc* seedlings growing on solid ATS medium, submerging the plants. Seedlings were vacuum infiltrated with *Agrobacterium* solution for 5 minutes and then

washed 5 times with sterile deionized water. Infiltrated seedlings were placed back into the growth chamber for 24 hours before collecting tissue for protein extraction.

***In vivo* immunoprecipitation and co-immunoprecipitation**

For co-immunoprecipitation assays, *35S::IBR5-Myc* seedlings transiently expressing HA-PAD1 were macerated in native extraction buffer (50 mM Tris-Cl, pH 7.5, 100 mM KCl, 10% glycerol, 0.1% Tween-20, 4 mM EGTA, 10 μ M MG132, 1 mM PMSF, and Protease Inhibitor Cocktail from Roche), incubated on a rocker for 10 minutes at 4°C, centrifuged at 10,000 x g for 10 minutes at 4°C, and the supernatant was collected. Protein was also collected from *35S::IBR5-Myc* seedlings to use as a negative control. Protein extracts were incubated with anti-HA agarose beads for 5 hours on a rocker at 4°C. Anti-HA agarose beads were pelleted by brief centrifugation, and the extract was completely removed with a narrow pipette tip. Beads were then washed 3 times for 3 minutes each with 500 μ l of Co-IP washing buffer (50 mM Tris-Cl, pH 7.5, 100 mM KCl, 10% glycerol, 0.05% Tween-20, 4 mM EGTA). Washing buffer was completely removed after the final wash with a narrow pipette tip, and anti-HA agarose beads were re-suspended in 15 μ l of 2X Laemmli sample buffer, and then boiled for 6 minutes in preparation for SDS-PAGE and western blot analysis.

SDS-PAGE and western blot analysis

Protein samples were run and separated by size via SDS-PAGE (Sodium dodecyl sulphate-polyacrylamide gel electrophoresis). Protein resolving gels were 10-14%

polyacrylamide, and electrophoresis of protein samples was performed in a protein running buffer (25 mM Tris-Cl, 192 mM glycine, 0.1% SDS [w/v]). Proteins of interest were transferred to polyvinylidene fluoride (PVDF) membranes (Bio-Rad) via wet electroblotting in cold transfer buffer (25 mM Tris-Cl, 192 mM glycine, 20% methanol [v/v], pH 8.3). PVDF membranes were then blocked with 5% non-fat milk/TBST solution (Tris buffered saline with Tween-20; 50 mM Tris-Cl, pH 8.0, 150 mM NaCl, 0.1% Tween-20) for 1-2 hours, and then washed 3 times for 5 minutes each with TBST. PVDF membranes were then incubated with primary antibody diluted in TBST (1:5,000 or 1:10,000 depending on protein levels) at room temperature for 1-2 hours or at 4°C for 4-18 hours (depending on protein levels) with gentle agitation. Membranes were then washed 3 times for 5 minutes each with TBST. Blots were incubated with corresponding secondary antibodies (1:10,000 dilutions in TBST) for 1-2 hours. Then the PVDF membranes were washed with TBST for 15 minutes, followed by 3 more 5 minute washes before proteins of interest were detected with enhanced chemiluminescence (ECL) plus kit (Bio-Rad) and exposure to autoradiography film (Gene Mate).

DNA isolation

DNA was isolated by grinding 10-30 mg of tissue (either whole seedlings or leaves) in 300 µl of 2X CTAB extraction buffer [2% cetyl trimethylammonium bromide (CTAB), 100 mM Tris-Cl (pH 8.0), 1.4 M NaCl, 20 mM EDTA], vortexing, and then heating the extract at 65°C for 10-30 minutes. Then 300 µl of chloroform was added to the samples, followed by brief vortexing and then centrifugation at 12,000 x g for 5 minutes. About 200 µl of each aqueous layer was collected and incubated with 600 µl of 100% ethanol at -20°C

for at least 30 minutes. DNA was pelleted by centrifugation at 16,000 x g for 20 minutes at 4° C. DNA pellets were then washed with 300 µl of 70% ethanol and centrifuged at 16,000 x g for 5 minutes at 4°C. All ethanol was removed and the DNA pellets were allowed to air dry before being re-suspended in 50-100 µl of 10 mM Tris-Cl (pH 8.0). Re-suspended DNA was stored at -20°C until ready for use.

Genotyping

The homozygous T-DNA mutant line for *pad1* was confirmed using T-DNA insert specific left border primer LB02 and gene specific primer PAD1 Sali R to detect the presence of the insert, and gene specific primers PAD1 BamHI F and PAD1 Sali R were used to confirm the interruption of the endogenous gene. LB02 and PAD2 F primers were used to detect the presence of the T-DNA insert in *pad2*, and PAD2 F and PAD2 DS R were used to confirm the interruption of the endogenous gene. To genotype *ibr5-1* mutants, PCR was performed using *ibr5-1 SnaB-F* and *ibr5-1 R* primers, adding an *SnaBI* cut site. Digestion with *SnaBI* produced a 447 bp fragment in WT and a 420 bp fragment in *ibr5-1*, which was resolved on a 3.5% agarose gel. Similarly, for *ibr5-4* genotyping, PCR was performed using *ibr5-4 F* and *ibr5-4 BsmAI R* primers, which added a *BsmAI* cut site. Digestion with *BsmAI* endonuclease produced a 249 bp fragment in WT and a 221 bp fragment in *ibr5-4*, which was observed after separating digestion products on a 3.5% agarose gel.

Table 1. Primer sequences.

Primer Name	Primer Sequence	Primer Length	T _m (°C)
PAD1 pENTR F	5'-CACCATGGCGAGATACGATCGAGCAAT-3'	27	68
pPAD1 pENTR F	5'-CACCGGTCAGGTAAGCTGATCAGAG-3'	25	64
PAD1 BamHI F	5'-AGGATCCAAGATGGCGAGATACGATC-3'	26	61
PAD1 SalI R	5'-GGTCGACTTCATGTTTCCTTCGCAG-3'	25	61
PAD1 D1 R	5'-AGGTCGACGTCCTCCAACGTAAGC-3'	25	64
PAD1 D3 F	5'-GGGATCCGACCCAGTTACTGTTGAG-3'	25	62
PAD1 D3 R	5'-AGTCGACATCATGGATCGGTCTGATAA-3'	27	60
PAD1 D5 F	5'-CGGATCCTCTGGTACATTCTCTGCTT-3'	26	61
PAD2 F	5'-CACCGAGATGGCTAGATACGATCGA-3'	25	63
PAD2 DS R	5'-AAGTTCAGATTGAGAAACAGAAACAG-3'	26	63
LB02 *	5'-TTGGGTGATGGTTCACGTAGTGGGCC-3'	26	75
ibr5-4 F **	5'-ACGGTTCCTATGTGCCAGAATCTC-3'	24	69
ibr5-4 BsmAI R **	5'-GAATGATAAATGTACTCACCTACTTGTC-3'	28	72
ibr5-1 SnB-F **	5'-GCCTGTTTCTTCCGATACGGTGGCTACG-3'	28	74
ibr5-1 R **	5'-ACATTAAGAACACGAGAGATTCCT-3'	24	63
qACTIN7-F***	5'-ATGGAAGTGGATGGTGAAGGC-3'	22	66
qACTIN7-R***	5'-GGACGACCAACAATACTTGGGAAC-3'	24	72
qSAUR9 F***	5'-TTCCAGTCACTCCTCCAAGTCC-3'	24	74
qSAUR9 R***	5'-AGGGATAGTGAGACCCATCTCGTG-3'	24	74
qGH3-3-F***	5'-TGGGACATCAGCTGGTGAAGG-3'	22	64
qGH3-3-R***	5'-TGTCTAATCCGGGCACGTAGAG-3'	22	58

*Designed by Salk Institute, **Designed by Sunethra Dharmasiri, ***Designed by Thilanka Jayaweera

Silique analysis

Mature siliques were collected from WT, *pad1*, *pad2*, and heterozygous *pad1/+ pad2/+* double mutant plants. Siliques were placed in a solution of 0.2 N NaOH and 1% SDS and left on a shaker overnight to clear the tissues. Silique analysis was performed on four separate occasions, each with similar results. In each trial, five to seven siliques were cleared and observed for each line. Data collected was combined for statistical analysis. Images were obtained using Nikon SMZ1500 stereomicroscope.

Pollen viability assays

Mature pollen grains were collected from WT, *pad1*, *pad2*, and heterozygous *pad1/+ pad2/+* double mutant plants, treated with Carnoy's fixative (60% ethanol, 30% chloroform, 10% acetic acid), and stained with Alexander's pollen viability stain (9.5% ethanol, 4% glacial acetic acid, 0.01% malachite green, 0.05% acid fuchsin, 0.005% Orange g, 25% glycerin). Three separate trials of pollen staining assays were performed. In each trial, about 80 pollen grains were observed for each line. All three trials provided similar data. These data were combined for statistical analysis. Images were obtained using Nikon Alphaphot 2-YS2 microscope.

Immunolocalization and confocal imaging

Co-localization of PAD1-GFP and IBR5-Myc was visualized by performing an immunolocalization assay for IBR5-Myc. Four day old seedlings with *35S::PAD1-GFP* and *35S::IBR5-Myc* were fixed by vacuum infiltrating with 1% paraformaldehyde solution (in PBS) for 5 minutes and then incubating at room temperature with gentle agitation for one hour. Seedlings were then washed three times for 10 minutes each with PBS, then washed twice for 10 minutes each with DI H₂O. Seedlings were then mounted onto adhesive slides, and water was allowed to evaporate at 37°C. Each seedling was surrounded by a thin layer of hydrophobic wax before beginning incubation steps on the microscope slides. Roots of each mounted seedling were rehydrated by incubation in PBS for 10 minutes. Cell walls were then degraded by 45 minutes of incubation in 2% Driselase solution (in PBS) at 37°C. Seedlings were then washed four times for 8 minutes each. The

cell membranes of each sample were made permeable by one hour of incubation in permeabilization solution (10% DMSO, 3% IGEPAL CA-630, in PBS). Seedlings were then washed six times for 8 minutes each, before incubation in the blocking solution (2% BSA fraction V, in PBS) for two hours at 37°C. Blocking solution was then removed and replaced by the α -Myc primary antibody solution (1:1200 dilution in 2% BSA/PBS solution). Samples were incubated with primary antibody solution overnight (about 14 hours) at 4°C. Seedlings were then washed six times for 8 minutes each before incubation with the α -mouse IgG (Cy5) secondary antibody solution (1:1200 dilution in 2% BSA/PBS solution). Samples were incubated in the secondary antibody solution for three hours at 37°C. The seedlings were then washed three times with PBS for 10 minutes each before DAPI counter-staining. Seedlings were incubated in a 1 μ g/mL DAPI solution (in PBS) for 15 minutes at 37°C. Seedlings were then washed four more times for 10 minutes each before all PBS was removed and the seedlings were covered with Permount (Thermo Fisher) mounting solution. The same immunolocalization and DAPI staining procedures were performed using WT root tissue, providing a negative control for Cy5 and GFP visualization. Fluorescence was visualized and images captured using an Olympus FV1000 confocal microscope with either a 40x lens (numerical aperture of 1.00) or a 60x lens (numerical aperture of 1.4).

Four day old WT, *ibr5-4*, *pad1*, and *ibr5-4 pad1* seedlings with the *35S::DII-Venus* reporter construct were acclimated to liquid ATS (0.5% sucrose) for 30 minutes before preparing wet mounts for observation of root tips. DII-Venus protein levels were observed using the 515 nm laser of an Olympus FV1000 confocal microscope. Images of DII-Venus levels represent Z-stack projections. DII-Venus protein levels were imaged on two separate

occasions and provided similar results, with the data presented here representing images acquired during one session.

Root growth assays

Surface sterilized WT, *ibr5-1*, *pad1*, *pad2*, and *pad1 ibr5-1* seeds were plated on ATS media containing 2,4-D (0 nM, 40 nM, 70 nM, and 100 nM) or IAA (0 nM and 70 nM) and grown for 8 days. Plates with IAA media were wrapped with two layers of yellow cellophane to reduce photodegradation of IAA. Primary roots were straightened and measured in millimeters with a ruler. Percent inhibition of primary root growth was calculated using the following formula (Lincoln et al., 1990).

$$\% \text{ inhibition} = [(\bar{Y}-\bar{X})/\bar{Y}] * 100\%$$

The following equation was used to calculate the standard error of percent inhibition.

$$SE = \frac{\bar{X}}{\bar{Y}} \sqrt{\frac{SD_x^2}{n_x \bar{X}^2} + \frac{SD_y^2}{n_y \bar{Y}^2}}$$

Where \bar{X} = average of inhibited root lengths

\bar{Y} = average of uninhibited root lengths

n_x = number of inhibited roots measured

n_y = number of uninhibited roots measured

SD_x = standard deviation of inhibited values

SD_y = standard deviation of uninhibited values

RNA isolation and RT-PCR analysis

For analysis of auxin inducible gene expression in Col-0, *ibr5-1*, *pad1*, and *pad1 ibr5-1* backgrounds, 6 day old seedlings were incubated in ATS with 5 μ M IAA for 1 hour alongside an mock treated control set of seedlings. Tissue was washed in milli-Q before flash freezing in liquid nitrogen. 30 mg of each tissue sample was ground directly in liquid nitrogen, and dissolved in 0.5 ml of Tri-reagent by vortexing. Samples were centrifuged for 10 minutes at 4° C and the supernatants were collected and left at room temperature for 10 minutes. 0.2 ml of chloroform was added and the samples were vortexed for 15 seconds. Extracts were left at room temperature for 15 minutes before centrifuging at 13,200 x g for 15 minutes at 4° C. The upper aqueous layer was collected and 0.5 ml of isopropanol was added to each sample. Extracts were left at room temperature for 10 minutes and then centrifuged at 13,200 x g for 10 minutes at 4° C. Supernatant was discarded and the RNA pellet was washed with 1.0 ml of 70% ethanol by vortexing. Samples were centrifuged at 7,500 x g for 5 minutes at 4° C and then all ethanol was removed and the pellets were allowed to air dry. RNA pellets were re-suspended in 25 μ l of DEPC water by warming to 55° C for 10 minutes. RNA was quantified using a NanoDrop 1000 Spectrophotometer. Transcript levels of specific auxin inducible genes were measured with qRT-PCR using a Bio-Rad CFX Connect Real-Time System. Relative expression levels were statistically analyzed with the comparative CT method in order to calculate the fold change in expression of each gene ($2^{-\Delta\Delta CT}$) relative to Col-0 and relative to untreated expression levels (Livak & Schmittgen, 2001). ACTIN7 was used as the reference gene for all relative gene expression analysis. Each reaction was run in triplicates, with the entire experiment having two biological replicates.

Histochemical staining

Four day old *HS::AXR3NT-GUS*, *HS::AXR3NT-GUS ibr5-4*, *HS::AXR3NT-GUS pad1*, and *HS::AXR3NT-GUS ibr5-4 pad1* seedlings were acclimated to liquid ATS (0.5% sucrose) for 1 hour before being transferred to pre-warmed liquid ATS and kept in a 37°C shaker for 2.5 hours. Seedlings were fixed after heat shock by vacuum infiltrating with GUS fixer solution (0.3% formaldehyde, 0.3 M mannitol, 10 mM 4-morpholineethanesulfonic acid (MES)) for 5 minutes and then gently shaking in 2 ml of GUS fixer solution for 30 minutes. Seedlings were washed two times for 10 minutes each in 2 ml of 100 mM phosphate buffer (pH 7.0). Seedlings were then vacuum infiltrated with GUS staining solution (0.1 M 5-bromo-4-chloro-3-indolyl-beta-D-glucuronide cyclohexylammonium (X-Gluc), 100 mM phosphate buffer (pH 7.0), 10 mM EDTA, 0.1% Triton X-100, 1 mM potassium ferricyanide, 1 mM potassium ferrocyanide) for 15 minutes before incubating in 2 ml of GUS staining solution overnight at 37°C. Images of GUS stained root tips were photographed with a Nikon SMZ1500 stereo microscope (Nikon, Melville, NY). AXR3NT-GUS analysis in these mutant backgrounds were performed three times with similar results.

Data analysis

Single factor analysis of variance (ANOVA) was used to compare primary root growth, root growth inhibition, and qRT-PCR data among different genotypes. VassarStats (www.vassarstats.net) was used for statistical computation.

CHAPTER III

RESULTS

IBR5 and PAD1 proteins physically interact

A yeast two-hybrid screening previously identified PAD1 as an IBR5-interacting protein (P. Kathare, unpublished). The interaction between PAD1 and IBR5 was tested *in vitro*, by first expressing N-terminal GST tagged PAD1 protein (GST-PAD1) in *E. coli*. GST-PAD1 was extracted and affinity purified using glutathione-agarose beads. GST-PAD1 proteins was then incubated with plant derived IBR5-Myc protein extract. Non-specifically bound proteins were washed from the glutathione beads and GST-PAD1 interacting proteins were resolved using SDS-PAGE. Western blot analysis using anti-Myc antibody revealed that IBR5-Myc was pulled down with GST-PAD1 (Figure 4). The presence of IBR5-Myc in the GST-PAD1 pull-down but not in the GST pull-down indicates that IBR5 specifically interacts with PAD1 *in vitro*.

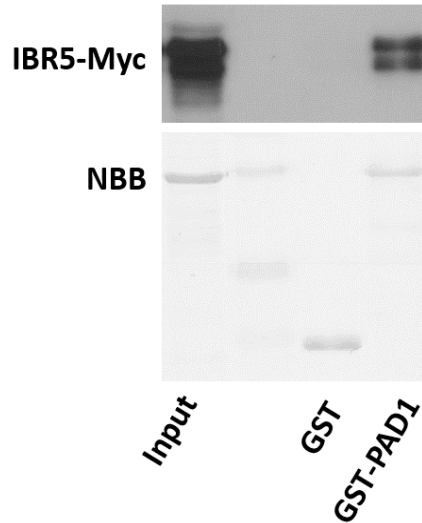


Figure 4. IBR5 interacts with PAD1 *in vitro*. Bacterially expressed GST and GST-PAD1 protein were isolated using glutathione-agarose beads and added to native protein extract from transgenic *Arabidopsis* seedlings expressing IBR5-Myc. Anti-Myc western blot analysis confirmed that IBR5-Myc was pulled-down with GST-PAD1. Protein blot stained with naphthol blue black (NBB) to visualize total protein. The second lane displays the PageRuler Plus protein ladder.

To elucidate the nature of the interaction between IBR5 and PAD1, pull-downs were performed with GST-PAD1 and various bacterially expressed IBR5-Myc truncated proteins. Truncated IBR5-Myc proteins (NT, F-box, ND1, D1, D2, D3, D4, and D6) were selected based on the domains of IBR5 which they contain, such as the F-box like domain, catalytic domain, and calmodulin binding domain (CBD) (Figure 5a). GST-PAD1 was extracted and affinity purified as described for the *in vitro* pull-down above. Glutathione bound GST-PAD1 was incubated with truncated IBR5-Myc proteins, expressed in and isolated from *E. coli*. Beads were washed and bound proteins were resolved using SDS-PAGE. Truncated IBR5-Myc proteins that interacted with GST-PAD1 were identified using anti-Myc western blot analysis (Figure 5b). Only truncated IBR5-Myc proteins containing the CBD were pulled down with GST-PAD1.

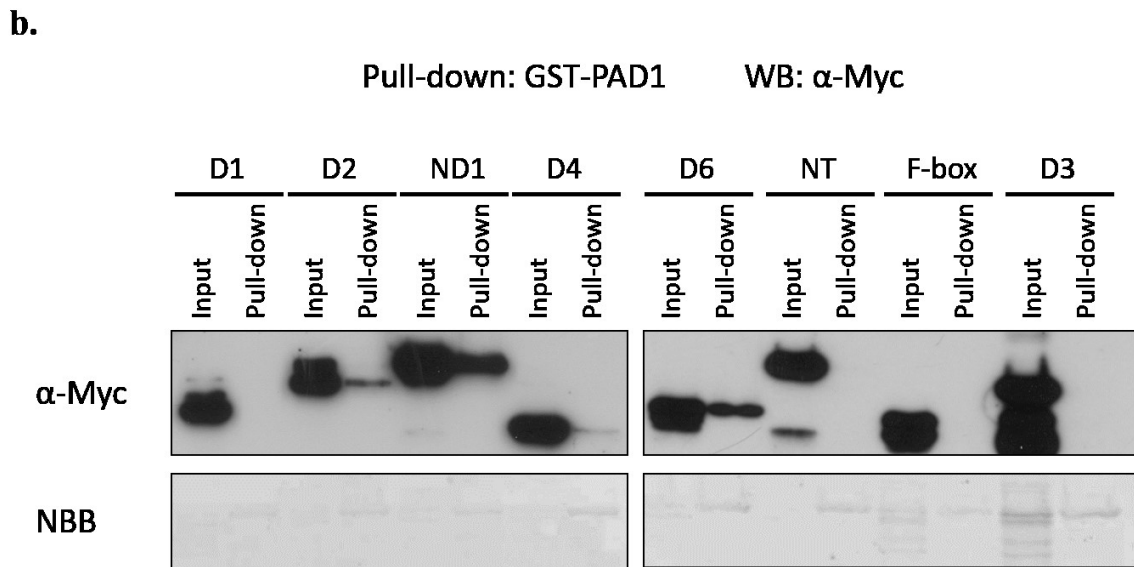
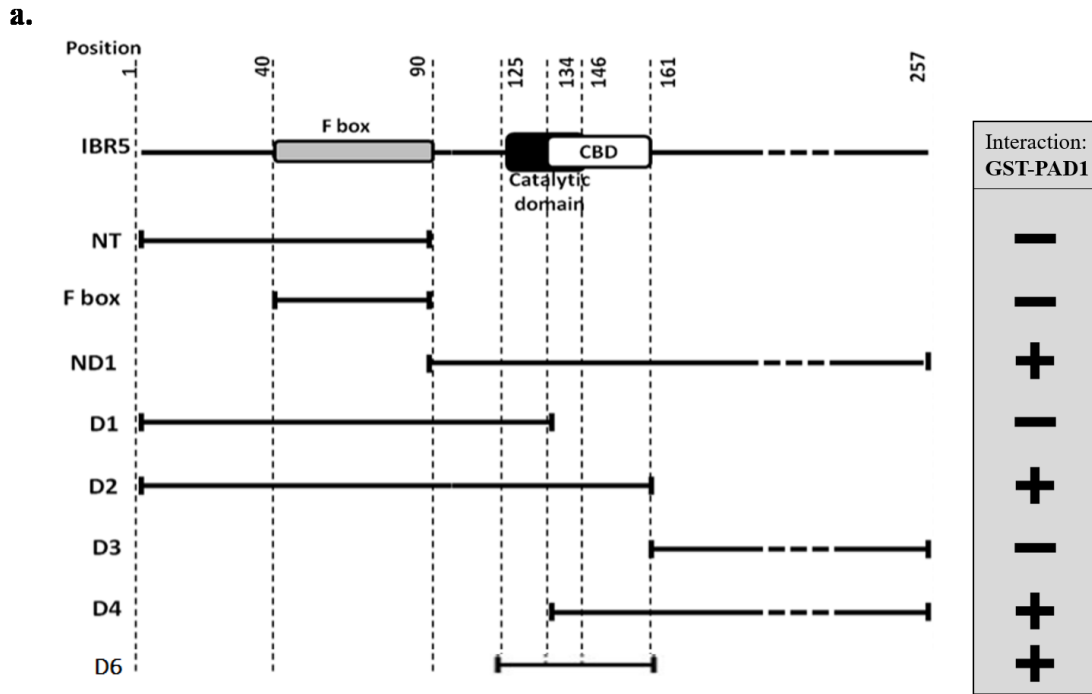


Figure 5. The CBD of IBR5 is required for interaction with PAD1. (a) IBR5-Myc truncated proteins arranged based upon which domains they contain. NT, F-box, D1, and D2 all contain the F-box like domain. ND1, D1, D2, D4, and D6 contain at least a portion of the catalytic domain. ND1, D2, D4, and D6 contain the CBD (calmodulin binding domain). (b) Anti-Myc western blot analysis of proteins pulled down with GST-PAD1, alongside respective inputs. Only truncated IBR5-Myc proteins with the CBD interacted with PAD1.

Pull-down assays with the truncated IBR5-Myc proteins indicated that the CBD and the catalytic domain may both be important for interaction with PAD1. It has also been shown that IBR5 interacts with several calmodulin proteins in the presence of Ca^{2+} (Jayaweera, unpublished). These results suggest that IBR5 could be involved in an interaction between CaMs and PAD1.

To further understand the interaction between IBR5 and PAD1, recombinant GST-PAD1 truncated proteins were bacterially expressed. GST-PAD1 D1, D2, and D3 truncated proteins, consisting of the first 100 residues (N-terminal portion), residues 101 through 151 (middle portion of PAD1), and the final 100 residues (C-terminal portion), respectively, were incubated with plant-derived IBR5-Myc protein extract. Pull down assays revealed that IBR5-Myc interacts predominantly with the GST-PAD1 D1 truncated protein, and to a lesser extent the GST-PAD1 D2 truncated protein, suggesting that the N-terminal portion of PAD1 is sufficient and necessary for interaction with IBR5 (Figure 6).

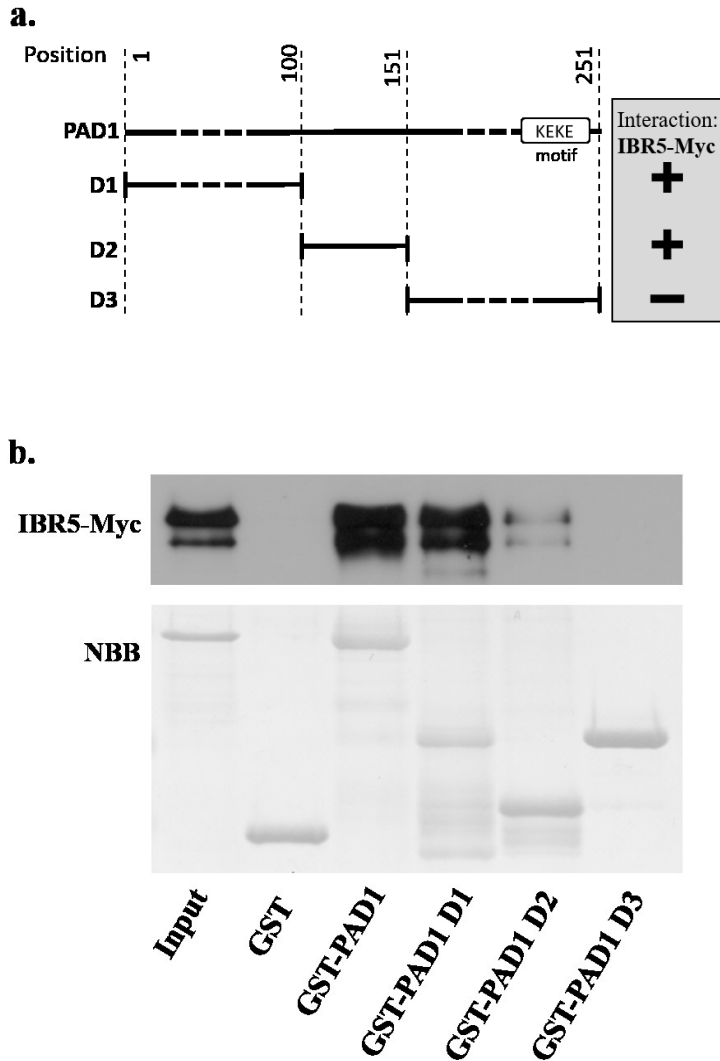


Figure 6. The N-terminal portion of PAD1 is required for interaction with IBR5. (a) Truncated GST-PAD1 proteins aligned with the full-length PAD1 protein. The “KEKE” motif represents a lysine and glutamate rich region. (b) Anti-Myc western blot analysis of proteins pulled down with GST-PAD1, and truncated PAD1 proteins. IBR5-Myc interacts strongly with the GST-PAD1 D1 truncated protein, and to a lesser extent the GST-PAD1 D2 truncated protein.

Since IBR5 and PAD1 interacted *in vitro*, *in vivo* co-immunoprecipitation of IBR5-Myc with HA-PAD1 was performed in order to confirm the interaction between IBR5 and PAD1. This experiment was done by expressing *35S::HA-PAD1* in four day old

35S::IBR5-Myc seedlings, using transient agrobacterium-mediated expression. Protein extracts from these seedlings were incubated with anti-HA agarose beads. Non-specifically bound proteins were washed away, and the remaining protein was resolved using SDS-PAGE. Anti-HA western analysis confirmed the immunoprecipitation of HA-PAD1, and anti-Myc western analysis confirmed that IBR5-Myc was co-immunoprecipitated (Figure 7). This finding suggests that PAD1 and IBR5 likely interact *in vivo*.

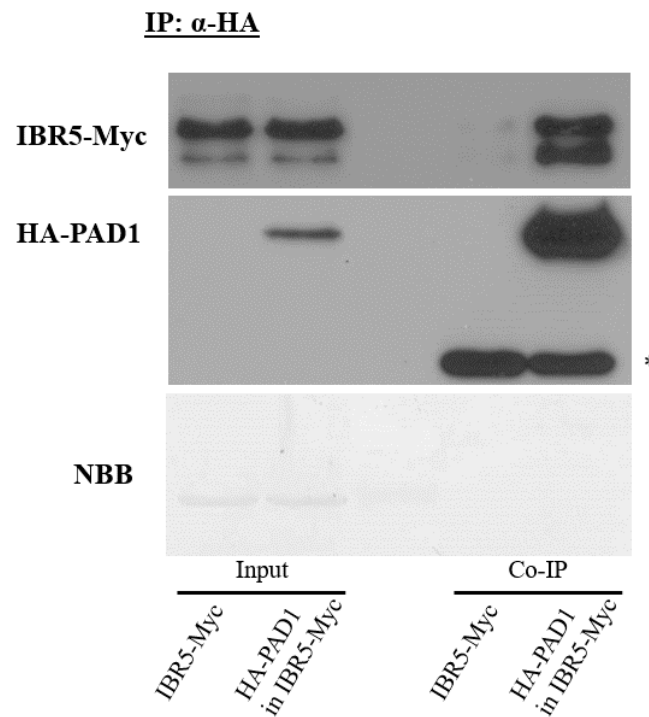
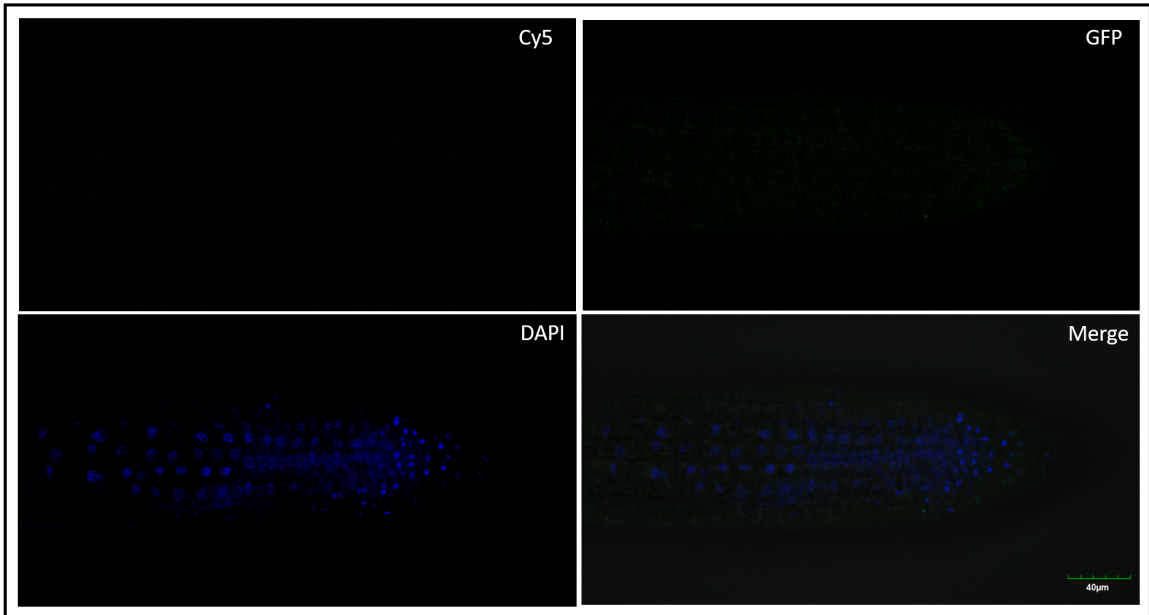


Figure 7. IBR5 interacts with PAD1 *in vivo*. Four day old IBR5-Myc seedlings were infiltrated with agrobacterium (GV3101) containing 35S::HA-PAD1. Equal amounts of IBR5-Myc and IBR5-Myc expressing HA-PAD1 were incubated with α -HA agarose beads in order to immunoprecipitate HA-PAD1. Anti-Myc western blot analysis revealed that IBR5-Myc was co-immunoprecipitated with HA-PAD1. “*” indicates non-specific protein binding of the anti-HA antibody. Co-immunoprecipitation of IBR5-Myc with HA-PAD1 was performed twice, with identical results.

Furthermore, a transgenic line with the translational reporter constructs *35S::PAD1-GFP* and *35S::IBR5-Myc* was used to determine whether PAD1 and IBR5 localize to the same subcellular location(s). IBR5-Myc was visualized using immunolocalization, with anti-mouse IgG secondary antibody conjugated to Cy5. Seedlings were stained with DAPI before observation in order to visualize nuclei. Root tissue of plants with *35S::PAD1-GFP* and *35S::IBR5-Myc* were observed using confocal microscopy. WT roots were used as a negative control to visualize the non-specific binding of antibodies during immunolocalization, and to visualize auto-fluorescence from the 488 nm laser (Figure 8a). IBR5-Myc was observed localizing to the cytoplasm and to the nucleus. PAD1-GFP was also observed in both the cytoplasm and the nucleus, but appeared to be present in much higher levels in the periphery of the nucleus and in the nucleolus (Figure 8b & 8c).

a. Negative Control



b.

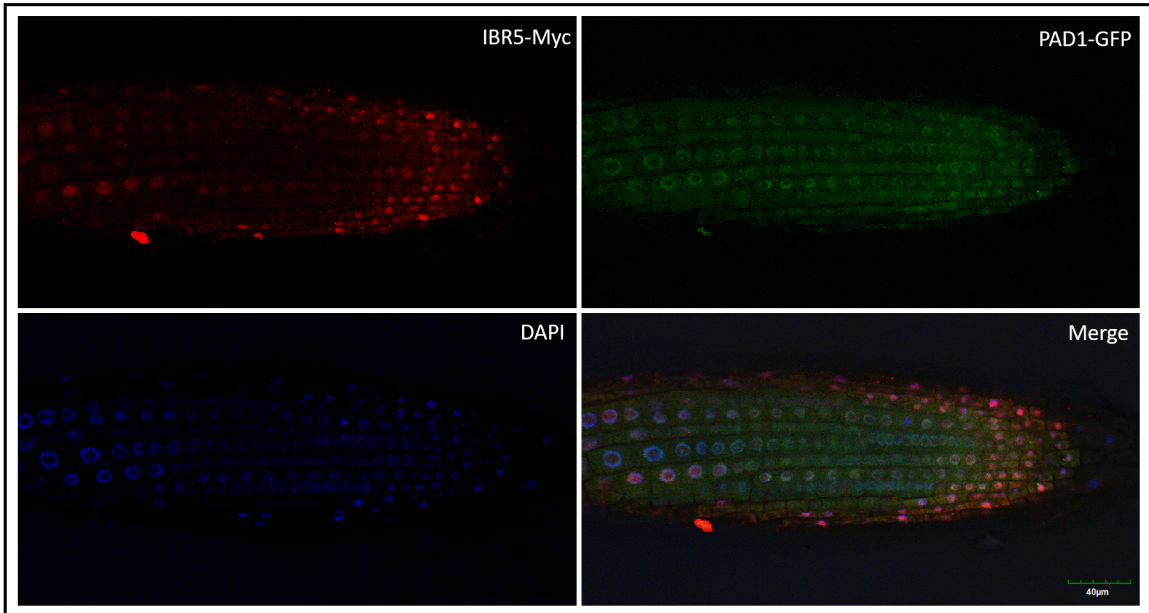


Figure 8. PAD1 and IBR5 co-localize to the cytosol and the nucleus.

C.

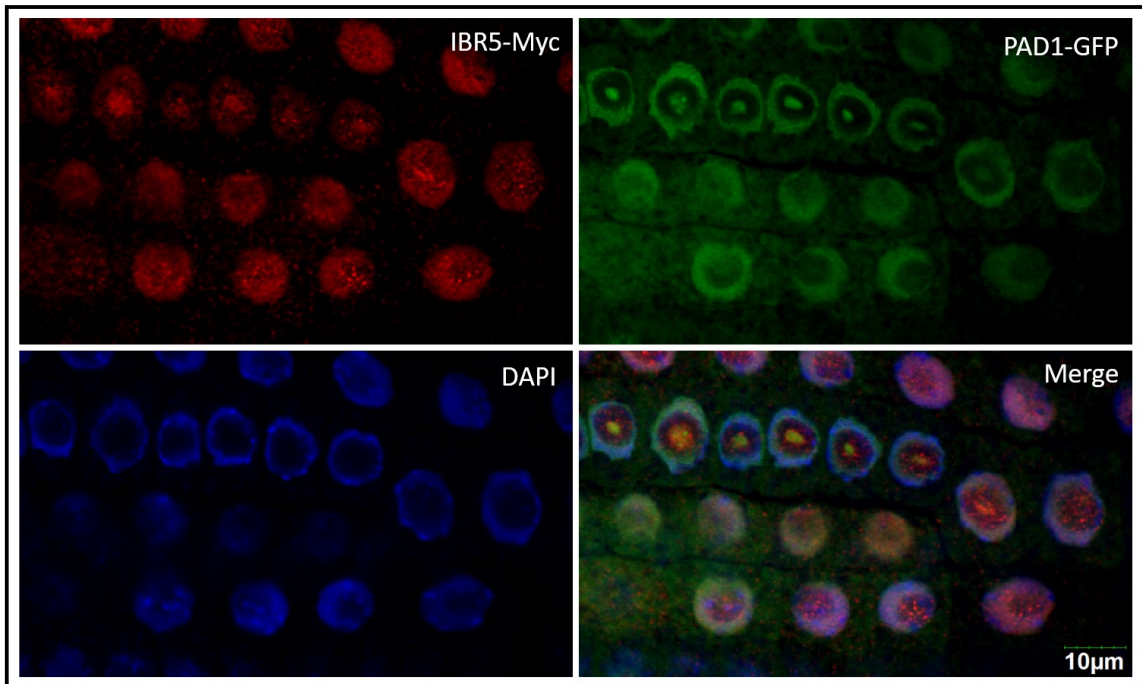


Figure 8 continued. PAD1 and IBR5 co-localize to the cytosol and the nucleus. Transgenic Arabidopsis plants expressing *35S::PAD1-GFP* and *35S::IBR5-Myc* were used to visualize the subcellular localization of each protein. (a) WT was used as a negative control to visualize background binding in the immunolocalization of IBR5-Myc (Cy5) and background auto-fluorescence using the 488 nm laser (GFP). (b) Image of immunolocalized IBR5-Myc, PAD1-GFP, and DAPI counter-staining acquired with a 40x lens. (c) Image of immunolocalized IBR5-Myc, PAD1-GFP, and DAPI counter-staining acquired with a 60x lens (image was also digitally magnified to 288% to focus on a smaller group of cells). IBR5-Myc appears to localize to the cytoplasm and to the nucleus. PAD1-GFP also appears to localize to the cytoplasm and the nucleus, however, there seems to be much more PAD1-GFP located in the periphery of the nucleus, as well as in the nucleolus. IBR5-Myc was visualized by immunolocalization, with anti-Myc primary antibodies and anti-mouse IgG secondary antibodies conjugated to Cy5. Seedlings were counter-stained with DAPI to visualize nuclei. Images were captured using an Olympus FV1000 confocal microscope.

***pad1* and *pad2* mutations are gamete lethal when combined**

The T-DNA mutants *pad1* (SALK_047984) and *pad2* (SALK_042314C) were obtained from the Arabidopsis Biological Resource Center (ABRC). The T-DNA insert in *pad1* is located in the second exon of the gene (Figure 9a). PCR was performed using the

PAD1 gene specific primers PAD1 BamH1 F and PAD1 Sal1 R, amplifying the gene from WT but not from the mutant. A second PCR was performed using the PAD1 Sal1 R and the T-DNA specific left border primer (LB02), amplifying the expected fragment from *pad1* but not from WT (Figure 9c). The T-DNA of *pad2* is located in the third exon (Figure 9b). The PAD2 gene specific primers PAD2 F and PAD2 DS R were used to amplify the gene from WT but not from *pad2*. Another PCR was performed using the PAD2 F and T-DNA LB02 primers, amplifying the expected fragment from *pad2* but not from WT (Figure 9c). These results confirm that both *pad1* and *pad2* T-DNA mutant lines are homozygous for the T-DNA insert.

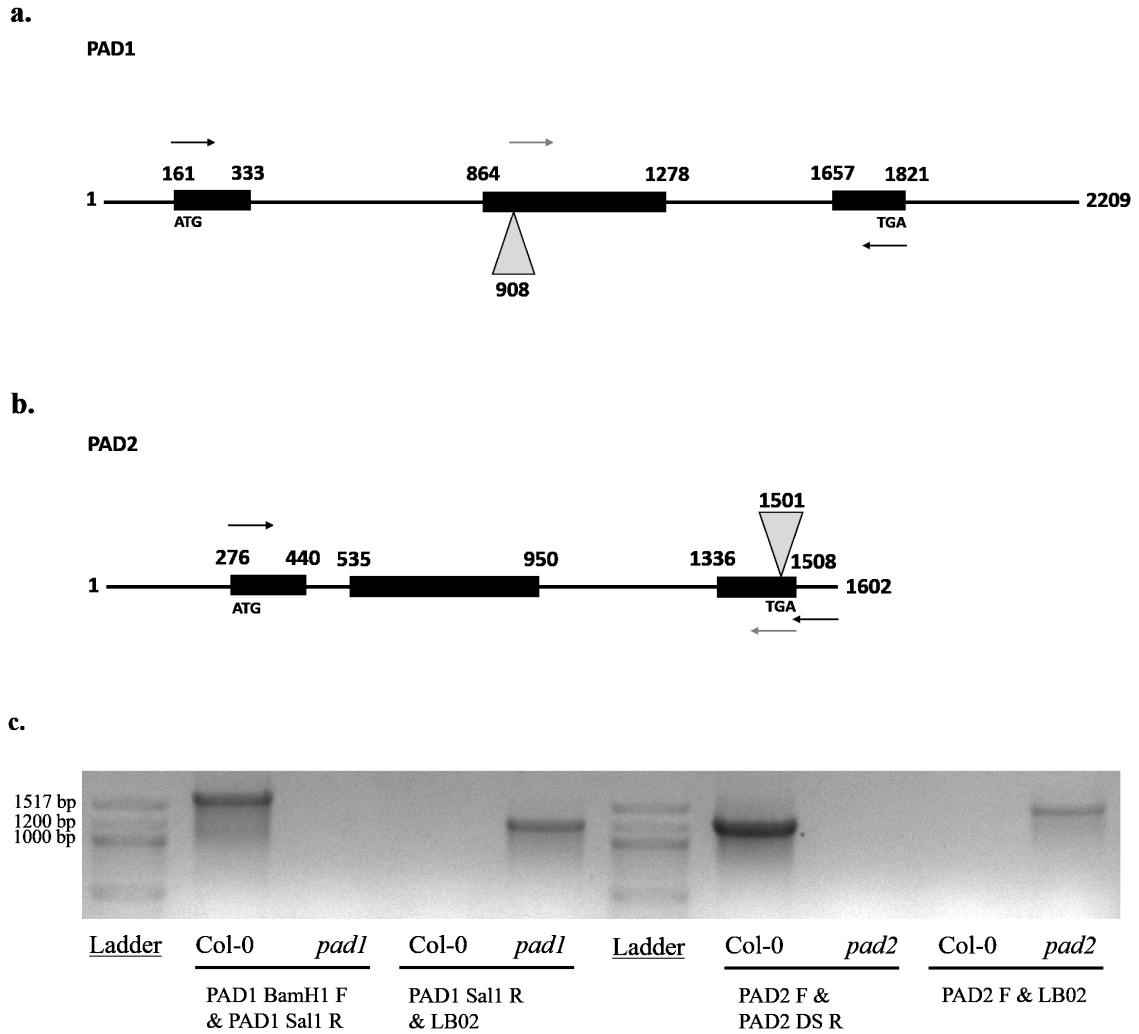


Figure 9. *pad1* and *pad2* T-DNA mutant lines are homozygous. (a) Schematic of the PAD1 gene and the location of the T-DNA insertion in the *pad1* mutant line. (b) Schematic of the PAD2 gene and the location of the T-DNA insertion in the *pad2* mutant line. T-DNA inserts are represented by grey arrows. Black rectangles represent exons, while the thin black lines represent introns and untranslated regions. Black arrows indicate the locations of gene specific forward and reverse primers, while grey arrows represent the T-DNA specific LB02 primer. (c) PAD1 specific primers amplify a 1660 bp fragment from WT, but not from *pad1* due to the T-DNA insertion. PAD1 Sal1 R and LB02 primers amplify a fragment representing the distance from the T-DNA insert to the end of the third exon. Similarly, PAD2 specific primers amplify a 1232 bp fragment from WT, but not from *pad2*. PAD2 F and LB02 primers amplify a fragment representing the distance from the T-DNA insert to the start site of the gene.

It is likely that PAD1 and PAD2 are functionally redundant, as their amino acid sequences are 95% identical (Fu et al., 1998). Therefore, an attempt was made to generate the higher order double mutant *pad1 pad2*. However, only heterozygous *pad1/+ pad2/+* double mutant lines could be identified, prompting investigation into the lethality of the double mutant. The siliques of *pad1/+ pad2/+* plants were observed for signs of aborted seeds. Siliques were collected from WT, *pad1*, *pad2*, and *pad1/+ pad2/+* plants, and tissues were cleared with a 0.2 N NaOH solution containing 1% SDS. Gaps within the siliques suggests that seed or ovule development is dysfunctional. These gaps were more prevalent in *pad1/+ pad2/+* siliques than in either of the single mutants or WT (Figure 10a). About 25% of the seeds within siliques from *pad1/+ pad2/+* plants were aborted, whereas only about 5% of seeds from WT, *pad1*, and *pad2* plants were aborted (Figure 10b). Pollen grains from the *pad1/+ pad2/+* plants' anthers were analyzed to investigate the likelihood of gamete lethality. Pollen grains were stained using Alexander's pollen viability stain. Inviability pollen grains, appearing light blue, were more abundant in *pad1/+ pad2/+* anthers as compared to either single mutant or WT (Figure 11a). About 25% of the pollen grains produced by double *pad1/+ pad2/+* plants are inviable, whereas only about 5% of pollen grains from WT, *pad1*, or *pad2* anthers were inviable (Figure 11b).

a.



b.

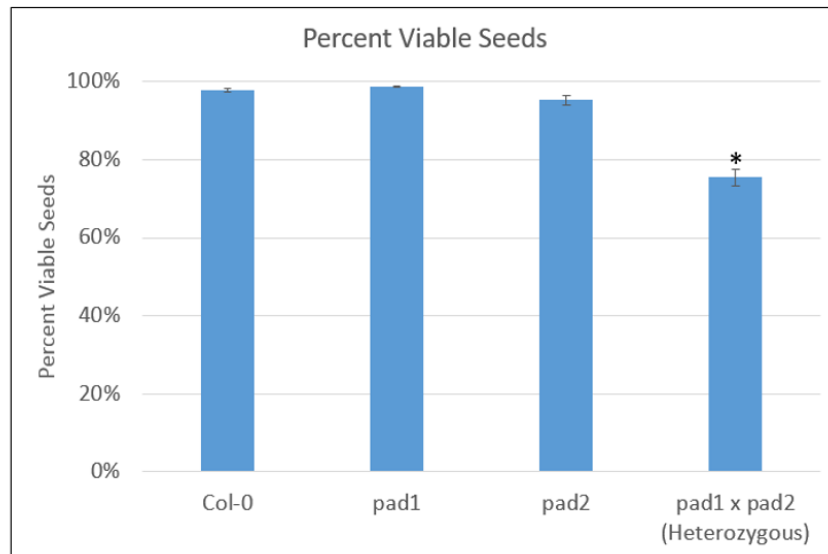


Figure 10. Heterozygous *pad1*+ *pad2*+ double mutants have fewer seeds within siliques. (a) Mature siliques were collected from WT, *pad1*, *pad2*, and *pad1*+ *pad2*+ plants. Siliques were placed in a solution of 0.2 N NaOH and 1% SDS and left on a shaker overnight to clear the tissues. There are noticeably more empty spaces within siliques from *pad1*+ *pad2*+ plants, likely due to inviability and early termination of female gametes. (b) Roughly one fourth of the seeds within *pad1*+ *pad2*+ siliques are terminated early; this ratio suggests that female gametes with *pad1* and *pad2* mutant genes are inviable. “*” indicates that the mean differs significantly from all other samples (WT, *pad1*, and *pad2*). $P < 0.05$, single factor ANOVA and Tukey’s HSD. Error bars represent standard deviations. Silique analysis was performed four times with similar results. Data presented is from one representative experiment.

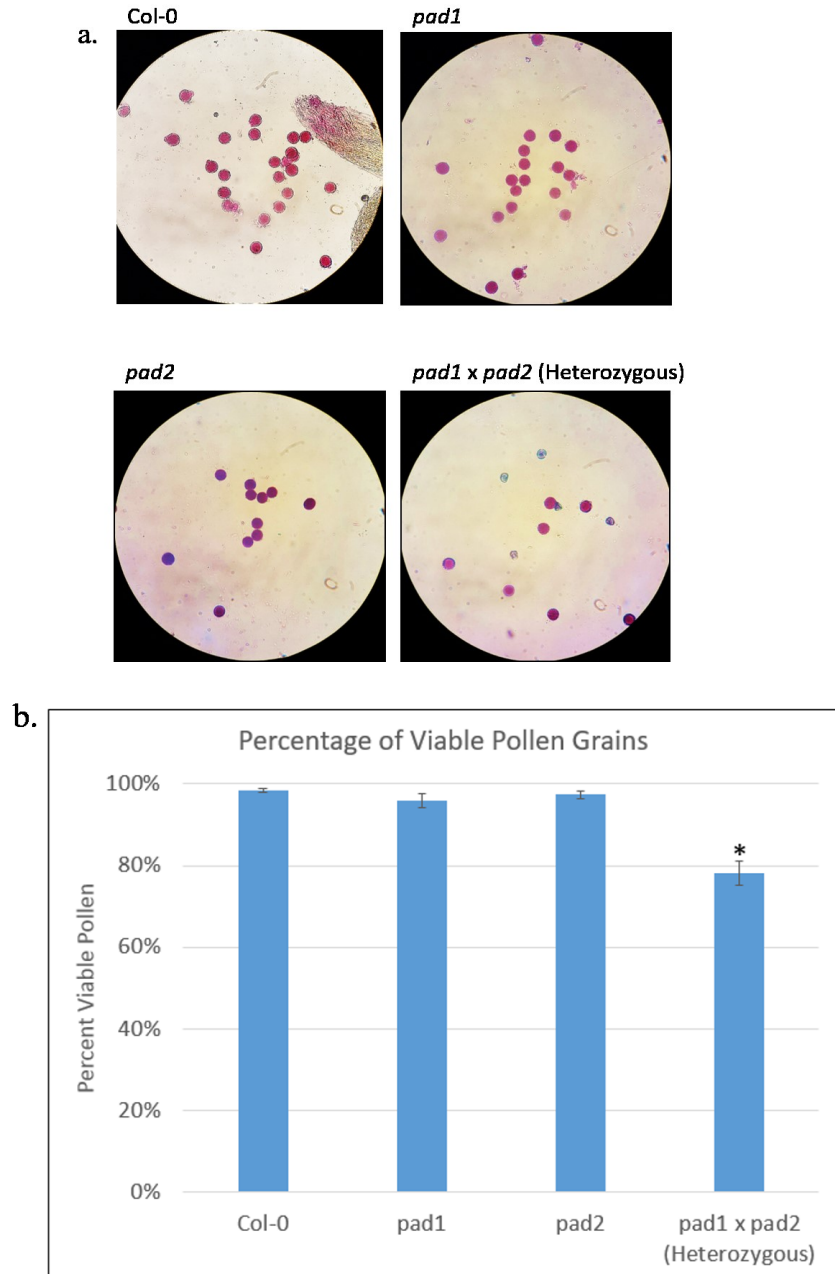


Figure 11. Heterozygous *pad1/+ pad2/+* plants produce significantly fewer viable pollen grains compared to WT or either single mutant. (a) Mature pollen grains were collected from each respective plant, treated with Carnoy's fixative, and stained with Alexander's pollen viability stain. Viable pollen grains appear dark red or magenta, while inviable pollen grains appear light blue. (b) Roughly one fourth of the pollen grains from *pad1/+ pad2/+* plants are inviable; this ratio indicates that male gametes with *pad1* and *pad2* mutant genes may be inviable. "*" indicates that the mean differs significantly from all other samples (WT, *pad1*, and *pad2*). $P < 0.05$, single factor ANOVA and Tukey's HSD. Error bars represent standard deviations. This pollen grain viability assay was performed three times with similar results. Data presented is from one representative experiment.

***pad1* and *ibr5-1* mutants exhibit resistance to exogenous auxin**

The *pad1* T-DNA mutant was crossed into the *ibr5-1* mutant background in order to investigate the auxin response in the *pad1 ibr5-1* double mutant. WT, *pad1*, *ibr5-1*, and the *pad1 ibr5-1* double mutant were grown on ATS medium containing various concentrations of the synthetic auxin 2,4-D. Relative to WT, the *pad1* and *ibr5-1* mutants had significantly longer primary roots after 8 days of growth on 2,4-D concentrations of 40 nM, 70 nM, and 100 nM, while the *pad1 ibr5-1* double mutant displayed an additive phenotype, with primary roots that were significantly longer than either of the parent mutants on all three 2,4-D concentrations (Figure 12). Additionally, the percentage inhibition of root elongation in each line was calculated for each concentration of 2,4-D. The *pad1 ibr5-1* double mutant and *ibr5-1* single mutant showed significantly less primary root growth inhibition as compared to WT on 40 nM, 70 nM, and 100 nM 2,4-D, while the *pad1* single mutant showed significant resistance on 70 nM and 100 nM 2,4-D as compared to WT (Figure 13). The *pad1 ibr5-1* double mutant showed significantly less primary root growth inhibition than either of the parent mutant lines on 70 nM and 100 nM 2,4-D (Figure 13).

Additionally, the *ibr5-1*, *pad1*, and *pad1 ibr5-1* mutants were grown on 70 nM IAA with similar results (Figure 14). The T-DNA mutant, *pad2*, was also analyzed for auxin-related phenotypes and was found to be resistant to 40 nM 2,4-D (Figure 15). Furthermore, recovery of the auxin-resistant *pad1* phenotype was observed in two independent *PAD1::PAD1-HA* transgenic lines (Figure 16). Resistance to auxins in mutants of *PAD1*, and its homolog *PAD2* further suggests a role in auxin signaling.

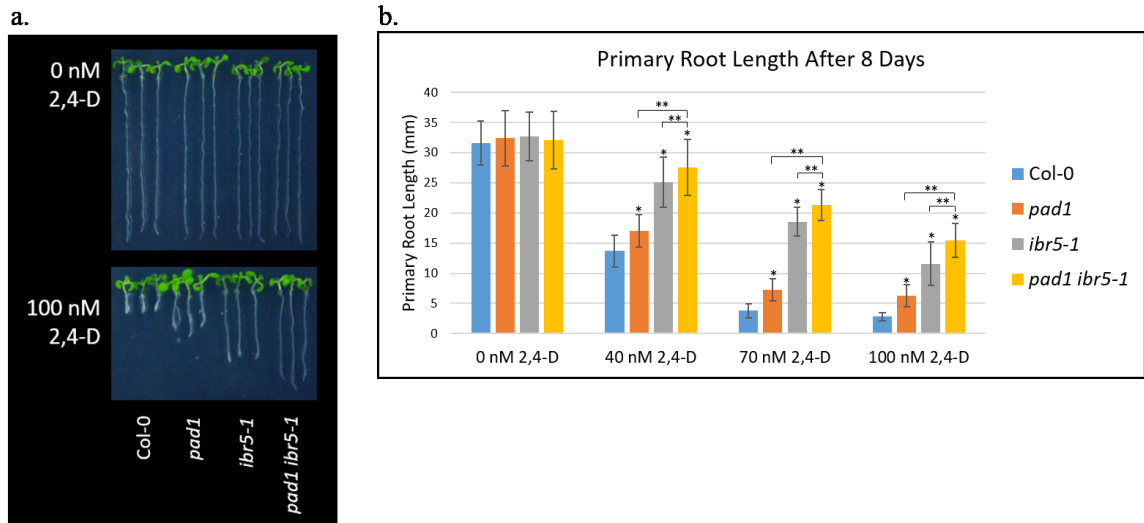


Figure 12. Primary roots of *pad1* and *ibr5-1* mutants are longer than WT roots when grown on 2,4-D. (a) The double mutant *pad1 ibr5-1* displays an additive phenotype on 2,4-D, with primary roots growing longer than either single mutant on 100 nM 2,4-D. (b) The double mutant *pad1 ibr5-1* displays an additive phenotype on 40 nM, 70 nM, and 100 nM 2,4-D. Seeds were plated directly onto ATS media containing the indicated concentrations of 2,4-D and grown at 22°C with constant light, for 8 days. “*” indicates that means differ significantly from WT. “**” indicates that the means differ significantly from each other. $P < 0.05$, single factor ANOVA and Tukey’s HSD. Error bars represent standard deviations. Root growth assay was repeated three times with similar results. Data presented is from one representative experiment.

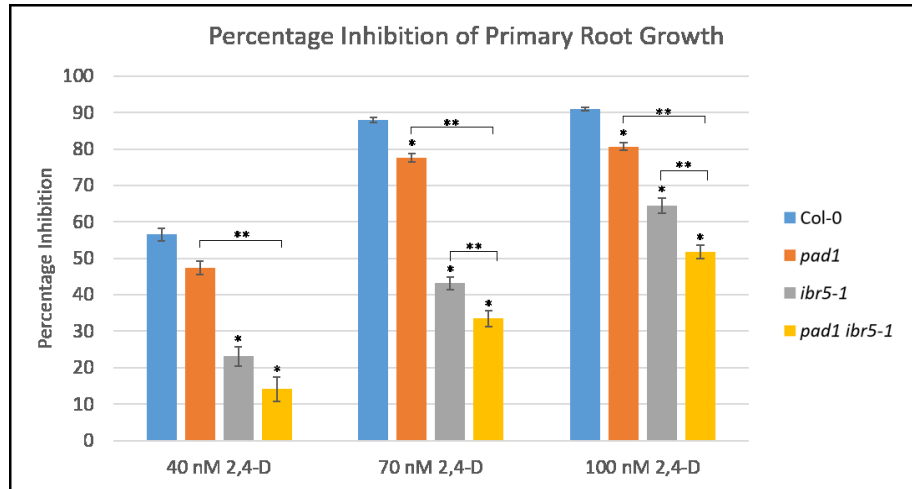


Figure 13. The *pad1 ibr5-1* double mutant is more resistant to primary root growth inhibition by 2,4-D than either of the *pad1* or *ibr5-1* single mutants. Primary root growth inhibition by 2,4-D of *pad1* and *ibr5-1* is significantly less as compared to WT. The double mutant, *pad1 ibr5-1* displays an additive phenotype, experiencing less root growth inhibition than either of the single mutants. “*” indicates that means differ significantly from WT. “**” indicates that the means differ significantly from each other. $P < 0.05$, single factor ANOVA and Tukey’s HSD. Error bars represent standard error. Root growth assay was repeated three times with similar results. Data presented is from one representative experiment.

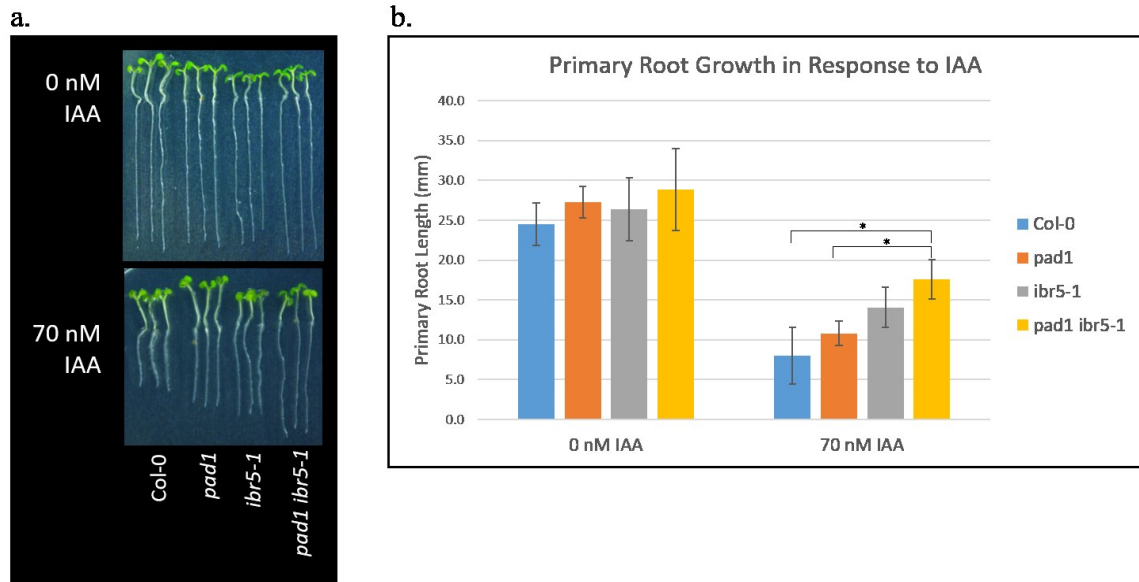


Figure 14. *pad1*, *ibr5-1*, and *pad1 ibr5-1* mutant lines are resistant to 70 nM IAA. Response of primary root growth to the natural auxin IAA is similar to that of the synthetic auxin 2,4-D. (a) Primary root length of each mutant line alongside WT, with representative seedlings selected from ATS plates containing either 0 nM IAA or 70 nM IAA. (b) Primary root length of the *pad1 ibr5-1* double mutant was significantly longer than that of WT and *pad1*. “*” indicates that the means differ significantly from each other. $P < 0.05$, single factor ANOVA and Tukey’s HSD. Error bars represent standard error. Root growth assay was repeated three times with similar results. Data presented is from one representative experiment.

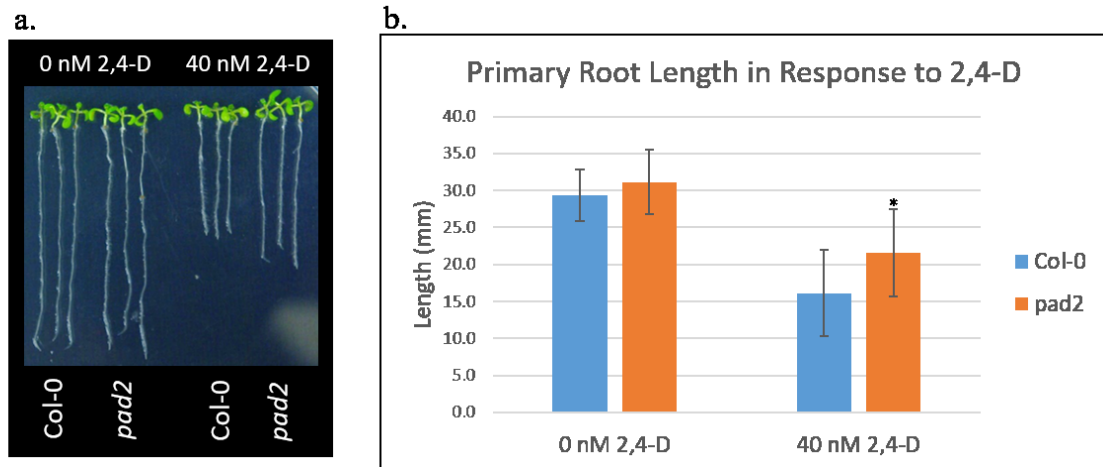


Figure 15. The *pad2* T-DNA mutant line displays an auxin-resistant phenotype. (a) Similar to the *pad1* mutant, *pad2* displays a resistance to auxin induced primary root growth inhibition. (b) *pad2* seedlings had significantly longer primary roots on 40 nM 2,4-D as compared to WT. “*” indicates that the mean differs significantly from WT on 40 nM 2,4-D. $P < 0.01$, single factor ANOVA and Tukey’s HSD used for statistical analysis. Error bars represent standard error. Root growth assay was repeated three times with similar results. Data presented is from one representative experiment.

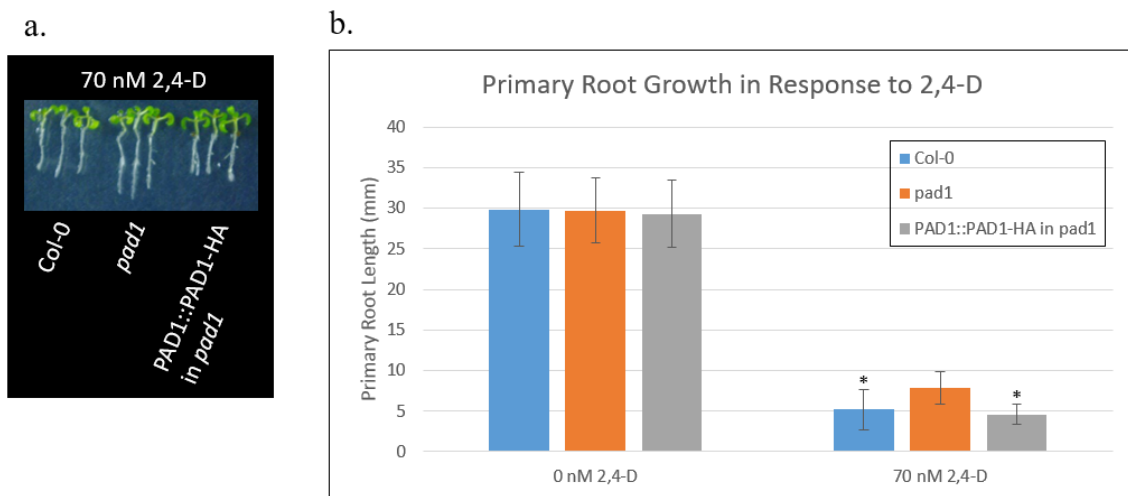


Figure 16. Expression of PAD1-HA in *pad1* mutant background recovers the mutant phenotype. (a) *pad1* seedlings grown on 70 nM 2,4-D display less primary root growth inhibition than the WT. Expression of PAD1::PAD1-HA in the *pad1* background recovers this mutant phenotype. (b) WT and PAD1::PAD1-HA in *pad1* seedlings had significantly shorter primary roots when grown on 70 nM 2,4-D. “*” indicates that the means differ significantly from the *pad1* mutant grown on 70 nM 2,4-D. $P < 0.01$, single factor ANOVA and Tukey’s HSD. Error bars represent standard error. Assay was repeated three times, and remained consistent among the two independent lines which were tested. Data presented is from one representative experiment.

***pad1* and *ibr5* mutations have contrasting effects on auxin responsive gene expression and Aux/IAA repressor protein degradation**

The auxin responsive genes *SAUR9* and *GH3.3* were selected for analysis in the WT, *ibr5-1*, *pad1*, and *ibr5-1 pad1* backgrounds. The expression of these two genes is highly inducible by auxin (Goda et al., 2008). RNA was isolated from mock treated seedlings and seedlings treated with 5 μ M IAA for 1 hour. Reverse transcription was used to generate cDNA, which was used in qRT-PCR to compare the relative expression levels and auxin-induced expression levels of *SAUR9* and *GH3.3* in the different mutant backgrounds. The relative expression levels of these two genes (Figure 17a), and their IAA-induced expression levels (Figure 17b), varied between the *ibr5-1*, *pad1*, and *ibr5-1 pad1* mutant backgrounds. However, the observed differences do not necessarily correlate with the observed auxin-resistant phenotypes of these mutants.

The reporter gene construct *HS::AXR3NT-GUS* was used to analyze Aux/IAA repressor protein levels in *ibr5-4*, *pad1*, and *ibr5-4 pad1* mutant backgrounds. AXR3NT-GUS levels were observed after heat shock and GUS staining. WT and *pad1* backgrounds showed similar levels of staining, while *ibr5-4* showed much lower levels of staining indicating that AXR3NT-GUS proteins are destabilized in *ibr5-4* (Figure 18). Interestingly, the AXR3NT-GUS destabilization is noticeably less in *ibr5-4 pad1* compared to *ibr5-4* (Figure 18).

Additionally, the reporter gene construct *35S::DII-Venus* was used to analyze Aux/IAA repressor protein levels in *ibr5-4*, *pad1*, and *ibr5-4 pad1* backgrounds. DII-Venus was slightly stabilized in the *pad1* mutant background, but unexpectedly, no noticeable difference was observed between WT, *ibr5-4*, and *ibr5-4 pad1* (Figure 19).

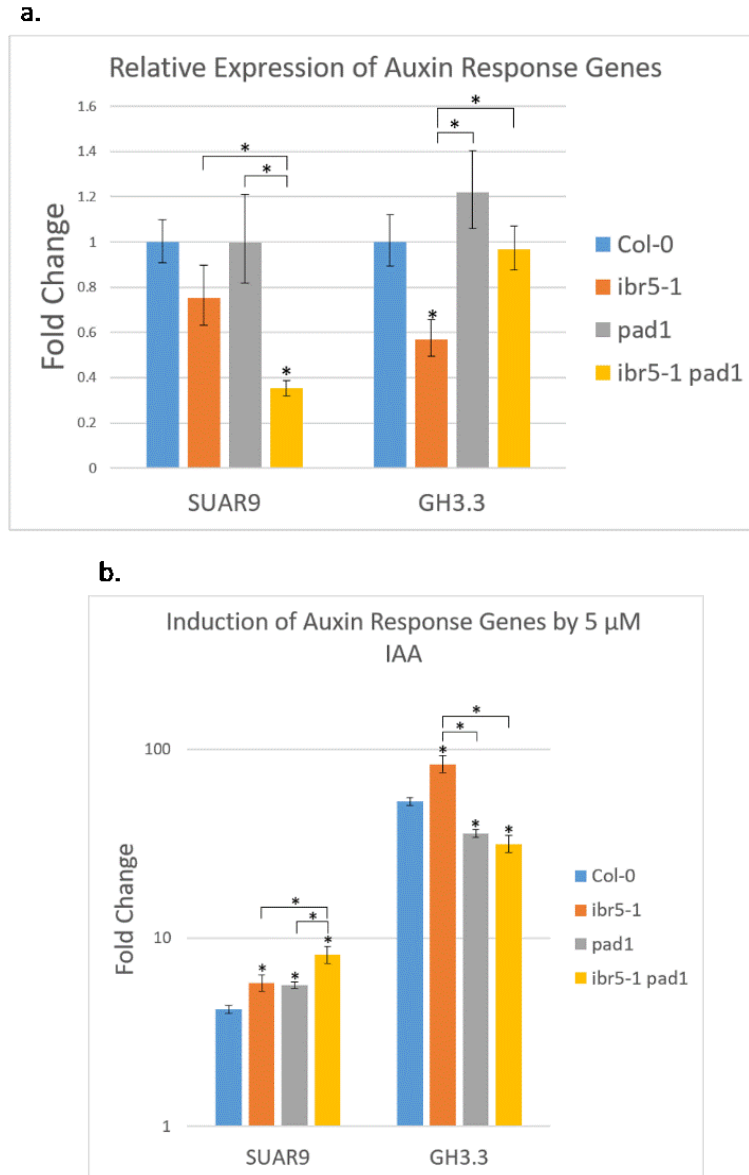


Figure 17. Auxin responsive gene expression is altered in *ibr5-1*, *pad1*, and *ibr5-1 pad1* mutants. (a) Compared to WT, *SAUR9* expression slightly less in *ibr5-1* and significantly less in *ibr5-1 pad1*. *SAUR9* expression in *ibr5-1 pad1* is significantly less than *ibr5-1* and *pad1* as well. Compared to WT, *GH3.3* expression is significantly less in *ibr5-1* and slightly more in *pad1*. *GH3.3* expression in *ibr5-1* is significantly less than *pad1* and *ibr5-1 pad1* as well. (b) Induction of *SAUR9* expression by IAA is significantly higher in *ibr5-1*, *pad1*, and *ibr5-1 pad1* compared to WT. *SAUR9* induction is significantly less in *ibr5-1* and *pad1* than in *ibr5-1 pad1*. Induction of *GH3.3* expression by IAA is significantly higher in *ibr5-1* and significantly lower in *pad1* and *ibr5-1 pad1*. *GH3.3* induction is significantly less in *pad1* and *ibr5-1 pad1* than in *ibr5-1*. Experiment was performed twice with similar results. The data presented is from one biological replicate.

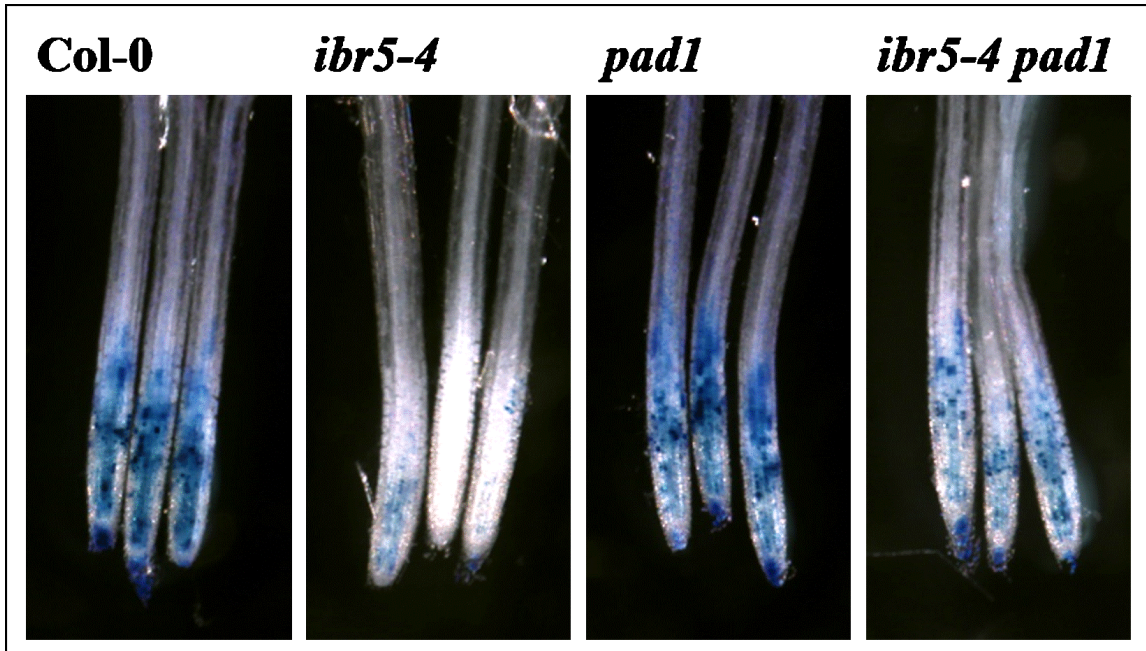


Figure 18. *pad1* partially recovers the AXR3NT-GUS destabilization in *ibr5-4*. AXR3NT-GUS expression was induced by heat shock and visualized by GUS staining. AXR3NT-GUS levels in WT are comparable with the levels in *pad1*. AXR3NT-GUS levels in *ibr5-4* are highly reduced, indicating destabilization of the protein. AXR3NT-GUS levels in *ibr5-4 pad1* are much less than WT or *pad1*, but noticeably higher than that of *ibr5-4*. AXR3NT-GUS analysis was performed three times with similar results.

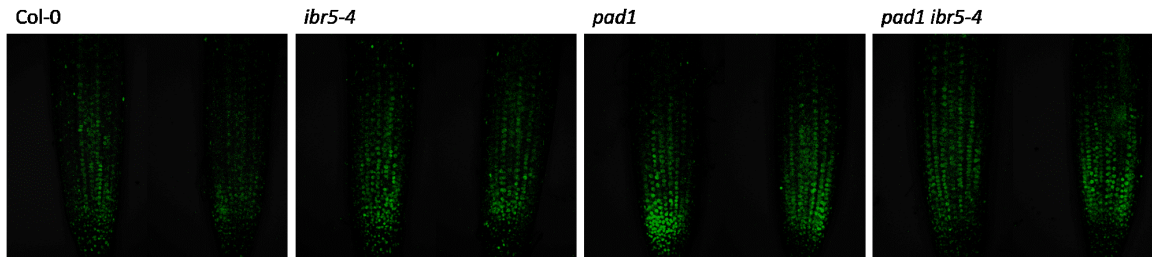


Figure 19. DII-Venus protein levels are slightly stabilized in *pad1*. DII-Venus protein levels are relatively equal in WT, *ibr5-4*, and *pad1 ibr5-4* backgrounds. There is a noticeable stabilization of DII-Venus levels *pad1*. Two photos of each lines are displayed in order to portray observed variation. Images represent Z-stack projections. Images were captured using an Olympus FV1000 confocal microscope

CHAPTER IV

DISCUSSION

IBR5 and PAD1 physically interact *in vitro* and *in vivo*

Elucidation of IBR5's role in the auxin signaling pathway prompted a yeast two-hybrid screening for IBR5-interacting proteins, resulting in the identification of the potential IBR5-interacting protein, PAD1 (P. Kathare, unpublished). This interaction was confirmed *in vitro* by pulling down plant-derived IBR5-Myc with recombinant GST-PAD1 (Figure 4). IBR5 was also shown to interact with PAD1 *in vivo* by co-immunoprecipitating IBR5-Myc protein with transiently expressed HA-PAD1 protein (Figure 7). Two isoforms of IBR5, IBR5.1 and IBR5.3, are transcribed due to alternative splicing (Jayaweera et al., 2014). IBR5.1 localizes to the cytoplasm and the nucleus, while IBR5.3 localizes to the nucleus only (Jayaweera et al., 2014). PAD1, as a component of the 26S proteasome, has been shown to localize to the ER, the cytoplasm, and the nucleus (Reits et al., 1997; Heazlewood et al., 2006). A transgenic line with PAD1-GFP and IBR5-Myc was used to visualize the subcellular localization of each protein. As expected, IBR5-Myc and PAD1-GFP were observed co-localizing to the nucleus and the cytoplasm, though PAD1-GFP was observed to localize more specifically to the periphery and nucleolus of the nucleus (Figure 8). Taken together, co-localization and physical interactions in yeast two-hybrid assays (data not shown), *in vitro* pull-down assays (figure 4), and *in vivo* co-immunoprecipitation assays (figure 7) strongly suggest that PAD1 is a true IBR5

interacting protein. Previous studies have suggested that IBR5 plays a role in regulating auxin response, a signaling pathway which utilizes the UPS (Strader et al., 2008, Jayaweera et al., 2014, Choi et al., 2014). This observation raises the possibility that the IBR5-PAD1 interaction may play an important role in the regulation of auxin signaling

As previously discussed, IBR5 is a dual specificity phosphatase that has been shown to interact with and dephosphorylate MPK12 (Lee et al., 2009). IBR5 also acts as a holdase, stabilizing CHS3 in conjunction with HSP90 and SGT1b (Liu et al., 2015). There are multiple other proteins identified in our lab with which IBR5 has been shown to interact (at least *in vitro*), including the SCF component ASK1 (T. Jayaweera, unpublished), CaM1, CaM3 (T. Jayaweera, unpublished), several GTPases (P. Ghimire, unpublished; E. Lopez, unpublished), and a subunit of the RNA Polymerase II complex (P. Kathare, unpublished). It is clear that IBR5 has multiple functions and may play a role in several cellular processes. The importance of the IBR5-PAD1 interaction is of particular interest, as the 26S proteasome is a central component in auxin signaling.

Characterization of the IBR5-PAD1 interaction

Potential interacting protein domains were identified in both IBR5 and PAD1 in order to characterize the physical interaction between these two proteins. A previous study identified 36 ASK1/2 interacting proteins by screening an Arabidopsis yeast two-hybrid library, 28 of which contained a conserved F-box motif (Risseuw et al., 2003). Though IBR5 does not contain an F-box motif, it does contain a region with noticeable similarity to an F-box motif. This “putative F-box motif” is 47% similar to the F-box consensus

sequence and 21% identical (T. Jayaweera, unpublished). Several of the identical amino acids have been shown to mediate direct physical interaction between SKP1 and F-box proteins (Schulman et al., 2000). This information along with preliminary results from our lab suggests that a putative F-box motif in IBR5 may be important for interaction with ASK1 (T. Jayaweera, unpublished). Additionally, IBR5 contains a calmodulin-binding domain (CBD) which overlaps with its catalytic domain (Jayaweera et al., unpublished). To test if any of these IBR5 domains were important for interaction with PAD1, pull-down assays were performed with GST-PAD1 and eight distinct IBR5-Myc truncated proteins expressed in *E. coli*. GST-PAD1 interacted with the IBR5-Myc ND1, D2, D4, and D6 truncated proteins, all of which contain the entire CBD and at least a portion of the catalytic domain (Figure 5).

Recent findings in our lab suggest that IBR5 interacts with the Ca^{2+} binding protein calmodulin (CaM1 and CaM3) in a Ca^{2+} -dependent manner (Jayaweera et al., unpublished). This interaction is mediated by the CBD of IBR5, which partially overlaps with the catalytic domain (T. Jayaweera et al., unpublished). It is not clear whether the CBD of IBR5 mediates the binding of CaM1 and PAD1 in complex, or if CaM1 and PAD1 compete for binding to IBR5. Furthermore, PAD1's interaction with IBR5's catalytic domain introduces the possibility for dephosphorylation of PAD1 by IBR5.

Phosphorylation of the proteasome has been a topic of interest for some time, and has been studied in a several model organisms (Tokumoto et al., 1999; Parmentiera et al., 1997; Masona et al., 1998; Guo et al., 2016). The phosphorylation state of the 20S CP and 26S proteasome is a dynamic and highly conserved mechanism for regulation of proteasome assembly and activity (Guo et al., 2017). The 20S CP of the proteasome is

capable of assembling into several larger complexes by interacting with different lid components including the 19S RP (Stadtmueller and Hill, 2011). The phosphorylation state of the 20S CP is important for association with different regulatory particles and activator complexes (Schmidt and Finley, 2014). In humans, protein kinase A (PKA) was found to directly interact with the 20S CP, resulting in increased peptidase activity (Lu et al., 2008). A similar study found that the phosphatase PP2A was also interacting with the 20S CP, and that inhibition of the phosphatase resulted in increased peptidase activity (Zong et al., 2006). PKA activity has also been shown to increase 26S proteasome assembly *in vivo* (Asai et al., 2009).

Previous research identified potential kinase substrate consensus sequences within PAD1, including consensus sequences for calcium/calmodulin-dependent kinase II, cAMP/cGMP-dependent kinase, casein kinase II, and tyrosine kinase (Parmentiera et al., 1997). PAD1 has also been shown to form a complex *in vitro* with Snf1-related protein kinases (SnRKs) and the SCF component ASK1, possibly involving PAD1's "KEKE" motif (Farrás et al., 2001). These kinase substrate consensus sequences, as well as the previously defined "KEKE" motif are areas of interest in the characterization of the IBR5-PAD1 interaction.

GST-PAD1 truncated proteins were generated in order to narrow the range of potential IBR5 interacting domains (Figure 6a). GST-PAD1 D1 consists of the first 100 amino acids, which includes several putative kinase substrate consensus sequences predicted by "The Arabidopsis Protein Phosphorylation Site Database" (Zulawski et al., 2013; Durek et al., 2010; Heazlewood et al., 2008), "NetPhos 3.1" (Blom et al., 2004), and "KinasePhos" (Huang et al., 2005) (Figure 20a). GST-PAD1 D2 consists of the next 51

amino acids; the middle portion of the protein. GST-PAD1 D3 consists of the remaining 100 amino acids, including the “KEKE” motif. *In vitro* pull-down assays were performed using plant-derived IBR5-Myc protein. IBR5-Myc interacted strongly with GST-PAD1 D1, weakly with GST-PAD1 D2, and not at all with GST-PAD1 D3 truncated proteins, indicating that the “KEKE” motif is likely not involved in this interaction (Figure 6b). In order to properly visualize the domains of PAD1 which interact with IBR5, a 3D model of PAD1 was generated using the SWISS-MODEL automated protein structure-modelling server, with the human 20S α 4 subunit used as the template model (Biasini et al., 2014; Bordoli et al., 2009; Arnold et al., 2006; Chen et al., 2016) (Figure 20b). GST-PAD1 D1 represents a region of PAD1 that begins with an N-terminal extension used for gate opening and closing of the 20S CP, followed by an α -helix that would be located on the exterior of the 20S CP (displayed as blue in Figure 20b) and would likely be involved in interactions with regulatory particles such as the 19S RP (Rabl et al., 2008; Förster et al., 2010). The protein structure continues with a β -hairpin that resides in the hydrophobic center of the protein, followed immediately by an extended loop region that protrudes outward (displayed as cyan in Figure 20b). This extended loop contains three potential kinase-specific phosphorylation sites at T51, S57, and S59 (Figure 20). The GST-PAD1 D1 construct ends with another β -hairpin that leads into an α -helix that interacts with the adjacent 20S α -subunit (Groll et al., 1997).

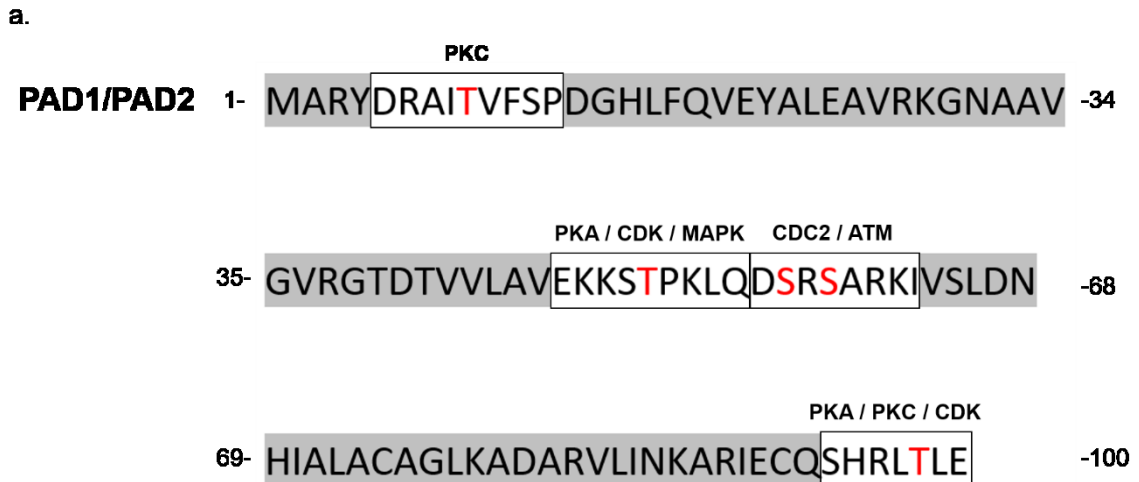


Figure 20. Putative phospho-sites of the proteasomal $\alpha 4$ subunit and 3D representation of PAD1. (a) The first 100 amino acid residues of PAD1 and PAD2, which are identical in this region of the protein. This portion of the protein is representative of the truncated GST-PAD1 DI protein. Putative phosphorylation sites are highlighted in red, and were determined by cross-referencing predicted phospho-sites from PhosPhAt 4.0, NetPhos 3.1, and KinasePhos. Only sites with confidence intervals $\geq 75\%$ were considered. The most likely kinases are included for each site based on kinase substrate consensus sequences. (b) Model of the Arabidopsis 20S proteasome $\alpha 4$ subunit, using the SWISS-MODEL automated protein structure-modelling server. The human 20S $\alpha 4$ subunit, modeled using electron microscopy, was used as a template. Ribbon model is color coded such that the N-terminus starts with blue and the C-terminus ends with red. Protein models generated using SWISS-MODEL are licensed under CC BY-SA 4.0 Creative Commons Attribution-ShareAlike 4.0 International License (<https://creativecommons.org/licenses/by-sa/4.0/legalcode>). Model observed using Open-Source PyMOL 1.3, PyMOL Molecular Graphics System (PyMOL™ Educational Product –Copyright © 2010 Schrodinger, LLC. For Educational Use Only).

Based on the information gathered from pull-downs with truncated PAD1 and IBR5 proteins, it can be suggested that IBR5's catalytic domain is directly interacting with some region within the PAD1 D1 truncated protein. There is a possibility, based on *in silico* investigation, that PAD1 has phosphorylation sites within this N-terminal region that are readily accessible to IBR5's phosphatase activity. It is tempting to suggest that reversible phosphorylation could act as a mechanism for regulating the assembly and/or activity of 26S proteasome. There is a precedent for this type of regulation, in which the human phosphatase UBLCP1 (the first and only proteasome phosphatase to be identified) was shown to dephosphorylate the 19S RP, promoting dissociation from the 20S CP (Guo et al., 2017; Sun et al., 2017).

Auxin-signaling is altered in IBR5 and PAD1 mutants

In order to gain insight into the relationship between IBR5 and PAD1, a T-DNA insertional mutant, *pad1*, was acquired and analyzed for auxin-related phenotypes. The *pad1* mutant displayed resistance to auxin-induced primary root growth inhibition, when using the synthetic auxin 2,4-D and when using the naturally occurring auxin IAA (Figures 12, 13, & 14). This phenotype was recovered by expressing *PAD1::PAD1-HA* in the *pad1* mutant (Figure 16). PAD1 has a homolog, PAD2, which is 95% identical at the amino acid level, so a T-DNA insertional mutant, *pad2*, was acquired for evaluation. The *pad2* mutant was found to be slightly but significantly resistant to auxin compared to WT, further confirming that the $\alpha 4$ subunit of the 20S proteasome is involved in auxin signaling (Figure 15). Given that both *pad1* and *pad2* mutants displayed similar auxin-resistant phenotypes, an attempt was made to generate a *pad1 pad2* double mutant. A previous study also

attempted to generate this higher order mutant using a different *pad1* T-DNA line (ABRC; GK-135D07) and a different *pad2* T-DNA line (ABRC; SALK_012558c), but failed to identify double homozygous mutants (Bolle et al., 2013). Our findings agree with this previous study, and furthermore we show that *pad1 pad2* double mutants cannot be isolated due to gamete inviability (Figures 13 & 14).

The double mutant *pad1 ibr5-1* was generated and grown alongside *ibr5-1* and *pad1* single mutants for comparison. The *pad1 ibr5-1* double mutant displayed a greater auxin-resistance than either *pad1* or *ibr5-1*, on both 2,4-D and IAA supplemented medium (Figures 15, 16, & 17). Phenotypic analysis of *pad1*, *pad2*, *ibr5-1*, and the *ibr5-1 pad1* double mutant revealed a similar auxin-resistant effect in each, with the double mutant showing an additive phenotype compared to either parent mutant. How this phenotypic effect is related to the physical interaction between IBR5 and PAD1 is not yet clear. An additive phenotype does not confirm a relationship between IBR5 and PAD1 in the auxin signaling pathway, but it is a likely scenario especially when considering the *in vivo* interaction between these two proteins.

The expression of two auxin response genes was analyzed to see whether there were changes in gene expression that might reflect the observed auxin-resistant phenotypes of *ibr5-1*, *pad1*, and *ibr5-1 pad1*. Expression of *SAUR9* and *GH3.3* was quantified in 4 day old seedlings using qRT-PCR. Expression of both of these genes was lower in *ibr5-1* than in WT, while expression in *pad1* is relatively equal to WT (Figure 17a). The expression of *SAUR9* in *ibr5-1 pad1* was significantly less than either *ibr5-1* or *pad1*, while *GH3.3* expression in *ibr5-1 pad1* was significantly higher than *ibr5-1* but slightly lower than *pad1* (Figure 17a). Additionally, the level of auxin-induced expression of these two genes was

measured with 4 day old seedling that had been treated for 1 hour with 5 μ M IAA. Induced expression of *SAUR9* was significantly higher in *ibr5-1*, *pad1*, and *ibr5-1 pad1* when compared with WT (Figure 17b). Induced expression of *SAUR9* in *ibr5-1 pad1* was significantly higher than either single mutant (Figure 17b). Induced expression of *GH3.3* in *ibr5-1* was significantly higher than WT, while *pad1* and *ibr5-4 pad1* lines showed significantly less expression compared to WT (Figure 17b). These data do not correlate with the observed auxin-resistant phenotypes of *ibr5-1*, *pad1*, and *ibr5-1 pad1*. However, this is a small representative group of genes which may not represent the general effects of these mutations on auxin responsive gene expression. It is also possible that IBR5 interacts with multiple components of the auxin signaling pathway, obscuring its effects.

Aux/IAA repressor protein degradation is altered in *pad1* and *ibr5-4* mutants

The *ibr5-1* and *ibr5-4* mutants have both been shown to have highly reduced levels of AXR3NT-GUS protein in the *HS::AXR3NT-GUS* reporter construct, which can be at least partially recovered by inhibition of the proteasome using MG132 (Strader et al., 2008; Jayaweera et al., 2014) suggesting that IBR5 negatively regulates Aux/IAA protein degradation. The *HS::AXR3NT-GUS* reporter construct was used to assess the stability of Aux/IAA repressor proteins in *pad1* and *ibr5-4 pad1* backgrounds. AXR3NT-GUS levels were relatively equal in WT and *pad1* root tips, while *ibr5-4* roots displayed the expected destabilization of AXR3NT-GUS (Figure 18). Interestingly, AXR3NT-GUS levels were noticeably higher in the *ibr5-4 pad1* double mutant compared with the *ibr5-4* levels, but still much lower compared to WT (Figure 18). This finding suggests that the *pad1* mutation partially recovers the destabilization of AXR3NT-GUS in *ibr5-4*.

The reporter construct *35S::DII-Venus* (derived from IAA28) was used in order to evaluate stability of the Aux/IAA DII domain in *ibr5-4*, *pad1*, and *ibr5-4 pad1*. Contrary to the destabilization of AXR3NT-GUS, DII-Venus levels in the root tip of *ibr5-4* seedlings appeared to be relatively equal to WT (Figure 19). DII-Venus appeared to be slightly stabilized in *pad1*, but was relatively equal to *ibr5-4* levels in the *ibr5-4 pad1* double mutant (Figure 19).

Both *HS::AXR3NT-GUS* and *35S::DII-Venus* reporter constructs have the DII degron motif responsible for Aux/IAA protein's interaction with F-Box proteins, but *HS::AXR3NT-GUS* also contains Domain I from the AXR3/IAA17 protein (Brunoud et al., 2012; Gray et al., 2001). It is possible that discrepancies in the stability of these proteins in *ibr5* mutants could be in some way attributed to the presence of Domain I in AXR3NT-GUS, or to differences in the rates of degradation between IAA17 and IAA28 proteins (Villalobos et al., 2012; Winkler et al., 2017).

Summary and future directions

Though numerous IBR5-interacting proteins have been identified, it is still not clear how IBR5 is involved in the regulation of auxin signaling. This work identified a novel interaction between IBR5 and the proteasome component PAD1. An *in vivo* interaction between these two proteins was demonstrated by co-immunoprecipitating IBR5-Myc with transiently expressed HA-PAD1 (Figure 7). Additionally, specific domains or regions of each protein were shown to be important for the interaction between IBR5 and PAD1 (Figures 5a & 6a). These findings suggest that IBR5's catalytic domain and/or its

calmodulin binding domain (CBD) are essential for interaction with PAD1 (Figure 5b). PAD1's N-terminal region was found to interact best with IBR5, implying that there is an important structural feature in this region which facilitates interaction with IBR5 (Figure 6b).

Mutants of *IBR5* and *PAD1* were found to have a similar auxin-resistant phenotype, exemplified in the additive phenotype of the *ibr5-1 pad1* double mutant (Figures 12, 13, & 14). There is a possibility that *IBR5* and *PAD1* function in parallel pathways within auxin signaling. However, IBR5 and PAD1 physically interact (Figure 7), and both localize to the nucleus (Figures 8), suggesting that the observed phenotypes may reflect a genetic interaction, and that IBR5 and PAD1 may be functioning within nuclear auxin signaling.

The stabilization of Aux/IAA repressor proteins was analyzed in *ibr5-4*, *pad1*, and *ibr5-4 pad1* mutant backgrounds. This analysis revealed a partial recovery of AXR3NT-GUS levels in *ibr5-4* when the *pad1* mutation is also present (Figure 18). However, analysis of DII-Venus levels in these same mutant backgrounds revealed discrepancies that cannot yet be fully explained (Figure 19).

This research has shown that IBR5 likely interacts *in vivo* with PAD1, that *ibr5* and *pad1* mutants have similar auxin-resistant phenotypes, and that destabilization of AXR3NT-GUS proteins in *ibr5-4* is partially recovered when combined with the *pad1* mutation. These findings, taken together with preliminary *in silico* investigation, may suggest a role for IBR5 in the reversible phosphorylation of PAD1 (Figure 20). This possibility is illustrated by a simple model in which normal 26S proteasome activity requires phosphorylation, and that when the proteasome is dephosphorylated (PAD1 for

instance) the activity is attenuated (Figure 21). This model suggests that the destabilization of AXR3NT-GUS in *ibr5* mutants may be due to hyper-phosphorylation of the proteasome

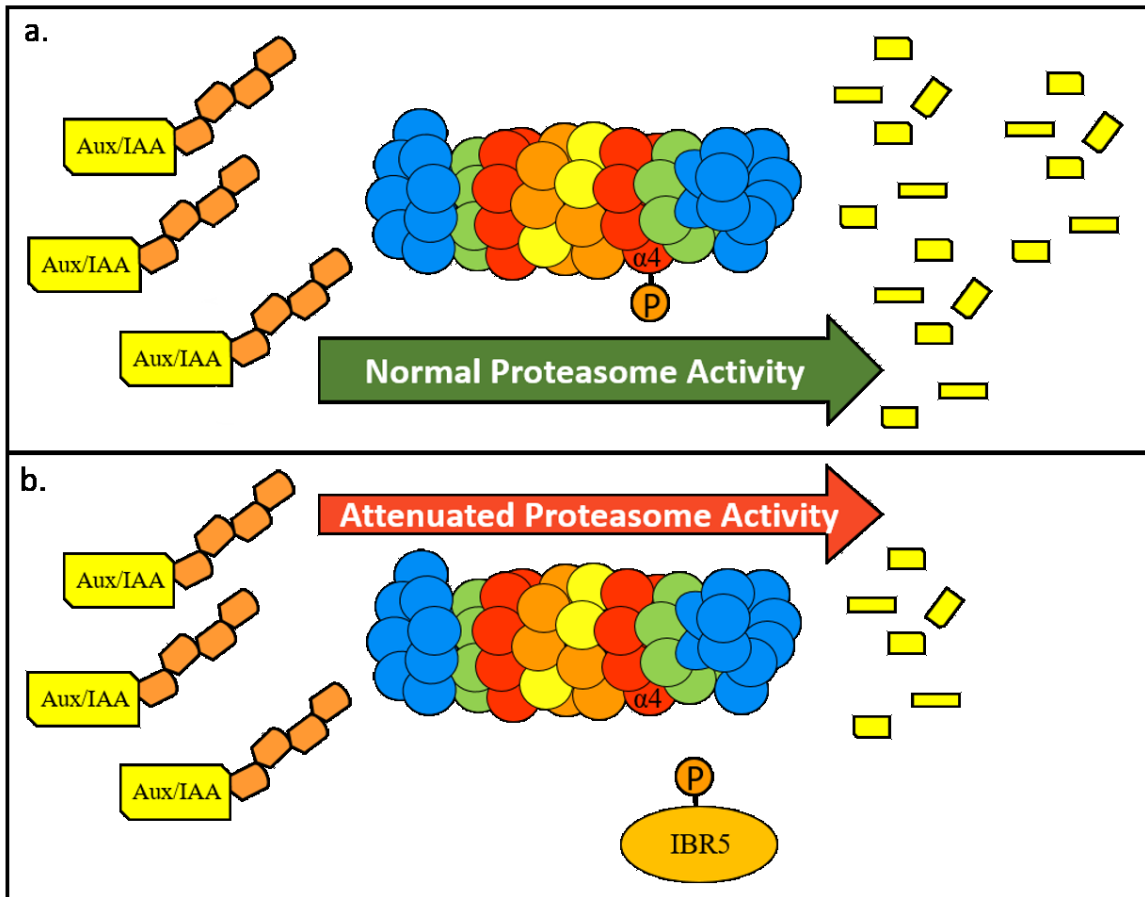


Figure 21. Reversible phosphorylation of PAD1 may regulate 26S proteasome activity. (a) If PAD1 is a phosphorylatable component of the 26S proteasome, its phosphorylation may promote the assembly and/or activity of the complex. (b) IBR5 may function to dephosphorylate PAD1, leading to a reduction in 26S proteasome activity.

leading to excess proteasome activity. This effect is partially recovered when a *pad1* mutation is introduced, since removal of this subunit would result in less phosphorylated proteasome residues. The partial recovery observed may be due to the presence of PAD2.

There is also the possibility that the PAD1-IBR5 interaction acts to recruit IBR5 to the proteasome to dephosphorylate a different protein. Previous findings from our lab agree with this model, specifically the stabilization of DII-Venus levels when IBR5 is overexpressed (data not shown; T. Jayaweera, unpublished). This model does not explain many of the findings related to the *ibr5* and *pad1* mutants however. The additive auxin-resistant phenotype and the auxin responsive gene expression data do not fit well into this model. Other mechanisms are likely affected by these mutations within the auxin signaling pathway. More work is required to understand how auxin response gene expression is regulated and how auxin-resistance occurs.

By studying known IBR5-interacting proteins and their relationships to the UPS, it is possible to begin to narrow the scope of potential points of regulation in which IBR5 may be functioning. HSP90, which has been shown to be involved in stabilization of the auxin receptor TIR1, has also been shown to interact with IBR5 (Wang et al., 2016; Liu et al., 2015). This connection is interesting, especially considering that both IBR5 (T. Jayaweera, unpublished) and TIR1 interact with ASK1 (Choi et al., 2014; Braun et al., 2011). How exactly HSP90 is involved in the regulation of SCF complexes is not clear, but there is evidence in yeast and in human cell lines that HSP90 is important for the regulation of 26S proteasome assembly and disassembly, as well as remodeling of CRLs in association with CSN sub-complexes (Imai et al., 2003; Nanduri et al., 2015; Manjarrez et al., 2014).

Regulated turnover of components within the UPS is essential for maintaining appropriate rates of degradation. The SCF complex undergoes cyclical regulation via the CSN, but much of this process is still unknown (Arnim, 2001; Zhang et al., 2008). The

SCF complex can be activated by neddylation, deactivated by deneddylation (via the CSN), and substrate receptor exchange can be mediated by CAND1 (Zhang et al., 2008). Mutations in CAND1 and the CSN result in attenuation of SCF activity, indicating that proper turnover of active and assembled SCF complexes is essential for their function (Arnim, 2001; Zhang et al., 2008). The 19S RP is structurally and functionally similar to the CSN, and it appears that both complexes are integral parts of the UPS. The 19S RP is responsible for processing polyubiquitinated substrates presented by the SCF complex, while the CSN is responsible for facilitating the turnover of SCF complexes (Förster et al., 2014; Cavadini et al., 2016). Furthermore, *in vitro* analysis suggests that the CSN competes with the 19S RP for binding to the 20S CP (Huang et al., 2005; Förster et al., 2014). There is also evidence that components of the SCF complex and components of the proteasome co-immunoprecipitate with the CSN (Feng et al., 2003). This evidence suggests that the CSN may be regulating the SCF complex in association with the proteasome.

The UPS is a highly regulated system, in which several large protein complexes work together to modulate the rate of degradation of specific and non-specific protein substrates. Regulation of the interactions between complexes such as the 20S CP, the 19S RP, HSP90, and the CSN is likely essential to the function of the UPS. Considering that all of these complexes have direct connections to CRL assembly, processing, and disassembly it is possible that IBR5 may be involved in the regulation of interactions between these complexes. Furthermore, this research suggests that PADI's interaction with, and possible dephosphorylation by, IBR5 could regulate the composition and activity of the 26S proteasome and in effect the UPS.

Moving forward, it will be critical to determine if PAD1 is phosphorylated, and if so, whether it is a substrate of IBR5. Other future directions for this research include a broader characterization of the *pad1* and *pad2* mutants. How these mutations affect the composition and activity of the 26S proteasome should be thoroughly characterized before the role in auxin signaling can be fully understood. A broader analysis of auxin response gene expression in *ibr5*, *pad1*, and *ibr5 pad1* double mutants may provide a deeper understanding of the roles of these proteins in auxin signaling. Furthermore, the stability of more Aux/IAA repressor proteins should be examined so that discrepancies can be addressed.

REFERENCES

- Abel, S., & Theologis, A. (1996). Early genes and auxin action. *Plant Physiology* 111(1), 9-17
- Abel, S., Oeller, P. W., & Theologis, A. (1994). Early auxin-induced genes encode short-lived nuclear proteins. *PNAS* 91(1), 326-330
- Arnim, A. G. (2001). A Hitchhiker's Guide to the Proteasome. *Sci. STKE* 97, pe2
- Arnold K., Bordoli L., Kopp J., and Schwede T. (2006). The SWISS-MODEL Workspace: A web-based environment for protein structure homology modelling. *Bioinformatics* 22, 195-201
- Asai, M., Tsukamoto, O., Minamino, T., Asanuma, H., Fujita, M., Asano, Y., Takahama, H., Sasaki, H., Higo, S., Asakura, M., Takashima, S., Hori, M., & Kitakaze, M. (2009). PKA rapidly enhances proteasome assembly and activity in in vivo canine hearts. *J Mol Cell Cardiol.* 46(4), 452-462
- Bartels, S., Besteiro, M. A. G., Lang, D., & Ulm, R. (2010). Emerging functions for plant MAP kinase phosphatases. *Trends in Plant Science* 15(6), 322-329
- Baumeister, W., Walz, J., Zühl, F., & Seemüller, E. (1998). The proteasome: paradigm of a self-compartmentalizing protease. *Cell* 92(3), 367-380
- Bedford, L., Paine, S., Sheppard, P. W., Mayer, R. J., & Roelofs, J. (2010). Assembly, structure, and function of the 26S proteasome. *Trends Cell Biol.* 20(7), 391-401

- Biasini M., Bienert S., Waterhouse A., Arnold K., Studer G., Schmidt T., Kiefer F., Cassarino T. G., Bertoni M., Bordoli L., Schwede T. (2014). SWISS-MODEL: modelling protein tertiary and quaternary structure using evolutionary information. *Nucleic Acids Research* 42(W1), W252-W258
- Blom N., Sicheritz-Ponten T., Gupta R., Gammeltoft S., Brunak S. (2004). Prediction of post-translational glycosylation and phosphorylation of proteins from the amino acid sequence. *Proteomics* 4(60), 1633-1649
- Bolle, C., Huep, G., Kleinbolting, N., Haberer, G., Mayer, K., Leister, D., & Weisshaar, B. (2013). GABI-DUPLO: a collection of double mutants to overcome genetic redundancy in *Arabidopsis thaliana*. *The Plant Journal* (2013) 75, 157-171
- Bordoli, L., Kiefer, F., Arnold, K., Benkert, P., Battey, J. and Schwede, T. (2009). Protein structure homology modelling using SWISS-MODEL Workspace. *Nature Protocols* 4(1)
- Bouché, N., Yellin, A., Snedden, W. A., & Fromm, H. (2005). Plant-specific calmodulin-binding proteins. *Annu. Rev. Plant Physiol.* 56, 435-466
- Braun, P., Carvunis, A.R., Charlotteaux, B., Dreze, M., Galli, M., & Vidal, M. (2011). Evidence for network evolution in an *Arabidopsis* interactome map. *Science* 333(6042), 601-607
- Brunoud, G., Wells, D. M., Oliva, M., Larrieu, A., Mirabet, V., Burrow, A. H., Beeckman, T., Kepinski, S., Traas, J., Bennett, M. J., & Vernoux, T. (2012). A novel sensor to map auxin response and distribution at high spatio-temporal resolution. *Nature Research Letter* 482, 103-108

- Bush, D. S. (1995). Calcium regulation in plant cells and its role in signaling. *Annu. Rev. Plant Physiol.* 46, 95-122
- Cavadini, S., Fischer, E. S., Bunker, R. D., Potenza, A., Lingaraju, G. M., Goldie, K. N., Mohamed, W. I., Faty, M., Petzold, G., Beckwith, R. E. J., Tichkule, R. B., Hasssiepen, U., Abdulrahman, W., Pantelic, R. S., Matsumoto, S., Sugasawa, K., Stahlberg, H., & Thomä, N. H. (2016). Cullin-RING ubiquitin E3 ligase regulation by the COP9 signalosome. *Nature* 531(7596), 598-603
- Chen, S., Wu, J., Lu, Y., Ma, Y. B., Lee, B. H., Yu, Z., Ouyang, Q., Finley, D. J., Kirschner, M. W., & Mao, Y. (2016). Structural basis for dynamic regulation of the human 26S proteasome. *Proc Natl Acad Sci U S A* 113(46), 12991-12996
- Chen, Y. H., & Kao, C. H. (2012). Calcium is involved in nitric oxide- and auxin-induced lateral root formation in rice. *Protoplasma* 249(1), 187-195
- Choi, C. M., Gray, W. M., Mooney, S., & Hellmann, H. (2014). Composition, roles, and regulation of Cullin-based ubiquitin E3 Ligases. *The American Society of Plant Biologists 2014*(The Arabidopsis Book), e0175
- Clough, S. J., & Bent, A. F. (1998). Floral dip: a simplified method for Agrobacterium-mediated transformation of Arabidopsis thaliana. *Plant J.* 16(6), 735-743
- Dharmasiri, N., Dharmasiri, S., & Estelle, M. (2005). The F-box protein TIR1 is an auxin receptor. *Nature* 435, 441-445

- Dharmasiri, S., Dharmasiri, N., Hellmann, H., & Estelle, M. (2003). The RUB/Nedd8 conjugation pathway is required for early development in Arabidopsis. *The EMBO Journal* 22(8), 1762-1770
- Dharmasiri, S., Jayaweera, T., & Dharmasiri, N. (2013). Plant hormone signaling: current perspectives on perception and mechanisms of action. *Ceylon Journal of Science*, 42(1), 1-17
- Durek, P., Schmidt, R., Heazlewood, J. L., Jones, A., MacLean, D., Nagel, A., Kersten, B., & Schulze, W. X. (2010). PhosPhAt: the Arabidopsis thaliana phosphorylation site database. An update. *Nucleic Acids Research* 38, D828-834
- Enders, T. A., & Strader, L. C. (2015). Auxin activity: past, present, and future. *American Journal of Botany*, 102(2), 180-196
- Farrás, R., Ferrando, A., Jásik, J., Kleinow, T., Ökrész, L., Tiburcio, A., ... & Koncz, C. (2001). SKP1-SnRK protein kinase interactions mediate proteasomal binding of a plant SCF ubiquitin ligase. *The EMBO Journal* 20(11), 2742-2756
- Feng, S., Ma, L., Wang, X., Xie, D., Dinesh-Kumar, S. P., Wei, N., & Deng, X. W. (2003). The COP9 signalosome interacts physically with SCF^{COII} and modulates jasmonate responses. *Plant Cell* 15(5), 1083-1094
- Förster, F., Lasker, K., Nickell, S., Sali, A., & Baumeister, W. (2010). Toward an integrated structural model of the 26S proteasome. *Molecular & Cellular Proteomics* 9.8, 1666-1677

- Förster, F., Schuller, J. M., Unverdorben, P., & Aufderheide, A. (2014). Emerging mechanistic insights into AAA complexes regulating proteasomal degradation. *Biomolecules* 4(3), 774-794
- Fu, H., Doelling, J. H., Arendt, C. S., Hochstrasser, M., & Vierstra, R. D. (1998). Molecular organization of the 20S proteasome gene family from *Arabidopsis thaliana*. *Genetics* 149, 677-692
- Fu, J., Yu, H., Li, X., Xiao, J., & Wang, S. (2011). Rice GH3 gene family. *Plant Signal Behav.* 6(4), 570-574
- Gallavotti, A. (2013). The role of auxin in shaping shoot architecture. *Journal of Experimental Botany* 64(9), 2593-2608
- Gil, P., & Green, P. J. (1996). Multiple regions of the *Arabidopsis* SAUR-AC1 gene control transcript abundance: the 3' untranslated region functions as an mRNA instability determinant. *The EMBO Journal* 15(7), 1678-1686
- Goda, H., Sasaki, E., Akiyama, K., Maruyama-Nakashita, A., Nakabayashi, K., Li, W., Ogawa, M., Yamauchi, Y., Preston, J., Aoki, K., Kiba, T., Takatsuto, S., Fujioka, S., Asami, T., Nakano, T., Kato, H., Mizuno, T., Sakakibara, H., Yamauchi, S., Nambara, E., Kamiya, Y., Takahashi, H., Hirai, M. Y., Sakurai, T., Shinozaki, K., Saito, K., Yoshida, S., & Shimada, Y. (2008). The AtGenExpress hormone and chemical treatment data set: experimental design, data evaluation, model data analysis and data access. *Plant J* 55(3), 526-542
- Gray, W. M. (2004). Hormonal regulation of plant growth and development. *PLOS Biology* 2(9), e311

- Gray, W. M., Kepinski, S., Rouse, D., Leyser, O., & Estelle, M. (2001). Auxin regulates SCF^{TIR1}-dependent degradation of AUX/IAA proteins. *Nature* 414, 271-276
- Groll, M., Ditzel, L., Löwe, J., Stock, D., Bochtler, M., Bartunik, H. D., & Huber, R. (1997). Structure of 20S proteasome from yeast at 2.4Å resolution. *Nature* 386, 463-471
- Guilfoyle, T. J., & Hagen, G. (2007). Auxin response factors. *Current Opinion in Plant Biology* 10, 453-460
- Guo, X., Huang, X., & Chen, M. J. (2017). Reversible phosphorylation of the 26S proteasome. *Protein Cell* 8(4), 255-272
- Guo, X., Wang, X., Wang, Z., Banerjee, S., Yang, J., Huang, L., & Dixon, J. E. (2016). Site-specific proteasome phosphorylation controls cell proliferation and tumorigenesis. *Nat Cell Biol.* 18(2), 202-212
- Gupta, R., Huang, Y., Kieber, J., & Luan, S. (1998). Identification of a dual-specificity phosphatase that inactivates a MAP kinase from Arabidopsis. *The Plant Journal* 16(5), 581-589
- Hagen, G., & Guilfoyle, T. (2002). Auxin-responsive gene expression: genes, promoters and regulatory factors. *Plant Molecular Biology* (49), 373-385
- Heazlewood, J. L., Durek, P., Hummel, J., Weckwerth, W., Walther, D., & Schulze, W. X. (2008). PhosPhAt: a database of phosphorylation sites in Arabidopsis thaliana and a plant-specific phosphorylation site predictor. *Nucleic Acids Research* 36, D1015-1021

- Heazlewood, J. L., Verboom, R. E., Tonti-Filippini, J., Small, I., & Millar, A. H. (2006). SUBA: the Arabidopsis subcellular database. *Nucleic Acids Research* 2007 (35), D213-D218
- Hepler, P. K., & Wayne, R. O. (1985). Calcium and plant development. *Annu. Rev. Plant Physiol.* 36, 397-439
- Huang, X., Hetfeld, B. K. J., Seifert, U., Kähne, T., Kloetzel, P. M., Naumann, M., Bechtolschir, D., & Dubiel, W. (2005). Consequences of COP9 signalosome and 26S proteasome interaction. *The FEBS Journal* 272(150), 3909-3917
- Huang, H. D., Lee, T. Y., Tseng, S. W., & Horng, J. T. (2005). KinasePhos: a web tool for identifying protein kinase-specific phosphorylation sites. *Nucleic Acids Research* 33, W226-229
- Imai, J., Maruya, M., Yashiroda, H., Yahara, I., & Tanaka, K. (2003). The molecular chaperone Hsp90 plays a role in the assembly and maintenance of the 26S proteasome. *The EMBO Journal* 22(14), 3557-3567
- Jayaweera, T., Siriwardana, C., Dharmasiri, S., Quint, M., Gray, W. M., & Dharmasiri, N. (2014). Alternative splicing of Arabidopsis IBR5 pre-mRNA generates two IBR5 isoforms with distinct and overlapping functions. *PLoS ONE* 9(8): e102301
- Kim, J., Harter, K., & Theologis, A. (1997). Protein-protein interactions among the Aux/IAA proteins. *PNAS* 94(22), 11786-11791

- Kipreos, E. T., & Pagano, M. (2000). The F-box protein family. *Genome Biology* 1(5), 3002.1-3002.7
- Knauss, S., Rohrmeier, T., & Lehle, L. (2003). The auxin-induced maize gene ZmSAUR2 encodes a short-lived nuclear protein expressed in elongating tissues. *The Journal of Biological Chemistry* 278(26), 23936-23943
- Kudla, J., Batistic, O., & Hashimoto, K. (2010). Calcium signals: the lead currency of plant information processing. *Plant Cell* 22(3), 541-563
- Lau, S., Shao, N., Bock, R., Jürgens, G., & Smet, I. D. (2009). Auxin signaling in algal lineages: fact or myth? *Trends in Plant Science* 14(4), 182-188
- Lee, J. S., Wang, S., Sritubtim, S., Chen, J. G., & Ellis, B. E. (2009). Arabidopsis mitogen-activated protein kinase MPK12 interacts with the MAPK phosphatase IBR5 and regulates auxin signaling. *The Plant Journal* (2009) 57, 975-985
- Li, Z. G., Chen, G. W., Li, Q. T., Tao, J. J., Bian, X. H., Ma, B., Zhang, W. K., Chen, S. Y., & Zhang, J. S. (2015). Three SAUR proteins SAUR76, SAUR77, and SAUR78 promote plant growth in Arabidopsis. *Scientific Reports* 5(12477), doi:10.1038/srep12477
- Lincoln, C., Britton, J. H., & Estelle, M. (1990). Growth and development of the axr1 mutants of Arabidopsis. *The Plant Cell* 2(11), 1071-1080
- Liu, J., Yang, H., Bao, F., Ao, K., Zhang, X., Zhang, Y., & Yang, S. (2015). IBR5 modulates temperature-dependent, R protein CHS3-mediated defense responses in Arabidopsis. *PLoS ONE Genetics* 11(0), e1005584

- Livak, K. J., & Schmittgen, T. D. (2001). Analysis of relative gene expression data using real-time quantitative PCR and the 2(-Delta Delta C(T)) method. *Methods* 25(4), 402-408
- Lu, H., Zong, C., Wang, Y., Young, G. W., Deng, N., Souda, P., Li, X., Whitelegge, J., Drews, O., Yang, P. Y., & Ping, P. (2008). Revealing the dynamics of the 20 S proteasome phosphoproteome. *Mol Cell Proteomics* 7(11), 2073-2089
- Makino, Y., Yoshida, T., Yogosawa, S., Tanaka, K., Muramatsu, M., & Tamura, T. (1999). Multiple mammalian proteasomal ATPases, but not proteasome itself, are associated with TATA-binding protein and a novel transcriptional activator, TIP120. *Genes to Cells* 4(9), 529-539
- Manjarrez, J. R., Sun, L., Prince, T., & Matts, R. L. (2014). Hsp90-dependent assembly of the DBC2/RhoBTB2-Cullin3 E3-ligase complex. *PLoS ONE* 9(3), e90054
- Mason, G. G. F., Murray, R. Z., Pappin, D., & Rivetta, A. J. (1998). Phosphorylation of ATPase subunits of the 26S proteasome. *FEBS Letters* 430(3), 269-274
- Monroe-Augustus, M., Zolman, B. K., & Bartel, B. (2003). IBR5, a dual-specificity phosphatase-like protein modulating auxin and abscisic acid responsiveness in Arabidopsis. *The Plant Cell* 15, 2979-2991
- Nagpal, P., Walker, L. M., Young, J. C., Sonawala, A., Timppe, C., Estelle, M., & Reed, J. W. (2000). AXR2 encodes a member of the Aux/IAA protein family. *Plant Physiol.* 123(2), 563-574

- Nakagawa, T. (2002). Gateway Binary Vector (pGWB). *Research Institute of Molecular Genetics (2002)*
- Nanduri, P., Hao, R., Fitzpatrick, T., & Yao, T. P. (2015). Chaperone-mediated 26S proteasome remodeling facilitates free K63 ubiquitin chain production and aggresome clearance. *J Biol Chem* 290(15), 9455-9464
- Newman, T. C., Ohme-Takagi, M., Taylor, C. B., & Green, P. J. (1993). DST sequences, highly conserved among plant SAUR genes, target reporter transcripts for rapid decay in tobacco. *Plant Cell* 5(6), 701-714
- Overvoorde, P., Fukaki, H., & Beeckman, T. (2010). Auxin control of root development. *Cold Spring Harb Perspect Biol* 2010 (2)
- Page, D. R., & Grossniklaus, U. (2002). The art and design of genetic screens: *Arabidopsis thaliana*. *Nature Reviews* 2002 (3), 124-136
- Parmentiera, Y., Bouchez, D., Flecka, J., & Genschika, P. (1997). The 20S proteasome gene family in *Arabidopsis thaliana*. *FEBS Letters* 416(3), 281-285
- Perochon, A., Aldon, D., Galaud, J. P., & Ranty, B. (2011). Calmodulin and calmodulin-like proteins in plant calcium signaling. *Biochimie*. 93(12), 2048-2053
- Popescu, S. C., Popescu, G. V., Bachan, S., Zhang, Z., Seay, M., Gerstein, M., Snyder, M., & Dinesh-Kumar, S. P. (2007). Differential binding of calmodulin-related proteins to their targets revealed through high-density *Arabidopsis* protein microarrays. *Proc Natl Acad Sci U S A*. 104(11), 4730-4735

- Rabl, J., Smith, D. M., Yu, Y., Chang, S. C., Goldberg, A. L., & Cheng, Y. (2008). Mechanism of gate opening in the 20S proteasome by the proteasomal ATPases. *Mol Cell* 30(3), 360-368
- Rayle, D. L., & Cleland, R. E. (1992). The acid growth theory of auxin-induced cell elongation is alive and well. *Plant Physiol.* 1992 (99), 1271-1274
- Realini, C., Rogers, S. W., & Rechsteiner, M. (1994). KEKE motifs: proposed roles in protein-protein association and presentation of peptides by MHC Class I receptors. *Federation of European Biochemical Societies Letters* (348), 109-113
- Reits, E. A., Benham, A. M., Plugastel, B., Neefjes, J., & Trowsdale, J. (1997). Dynamics of proteasome distribution in living cells. *The EMBO Journal* 16(20), 6087-6094
- Ren, H., & Gray, W. M. (2015). SAUR proteins as effectors of hormonal and environmental signals in plant growth. *Mol Plant.* 8(8), 1153-1164
- Risseuw, E. P., Daskalchuk, T. E., Banks, T. W., Liu, E., Cotelesage, J., Hellmann, H., Estelle, M., Somers, D. E., & Crosby, W. L. (2003). Protein interaction analysis of SCF ubiquitin E3 ligase subunits from Arabidopsis. *The Plant Journal* 34(6), 753-767
- Rogg, L. E., Lasswell, J., & Bartel, B. (2001). A gain-of-function mutation in IAA28 suppresses lateral root development. *The Plant Cell* (13), 465-480
- Schmid et al. (2005). Gene expression map of Arabidopsis development. *Nat. Gen.* 37,

- Schmidt, M., Finley, D. (2014). Regulation of proteasome activity in health and disease. *Biochim Biophys Acta*. 1843(1), doi:10.1016/j.bbamcr.2013.08.012
- Schulman, B. A., Carrano, A. C., Jeffrey, P. D., Bowen, Z., Kinnucan, E. R., Finnin, M. S., Elledge, S. J., Harper, J. W., Pagano, M., & Pavletich, N. P. (2000). Insights into SCF ubiquitin ligases from the structure of the Skp1-Skp2 complex. *Nature* 408(6810), 381-386
- Shimizu-Mitao, Y., & Kakimoto, T. (2014). Auxin sensitivities of all arabidopsis Aux/IAAs for degradation in the presence of every TIR1/AFB. *Plant & Cell Physiology* 55(8), 1450-1459
- Simon, S., & Petrášek, J. (2011). Why plants need more than one type of auxin. *Plant Science* 180(3), 454-460
- Simon, S., Kubeš, M., Baster, P., Robert, S., Bobrev, P. I., Friml, J., Petrášek, J., & Zažímalová, E. (2013). Defining the selectivity of processes along the auxin response chain: a study using auxin analogues. *New Phytologist* 200(4), 1034-1048
- Spiess, G. M., Hausman, A., Yu, P., Cohen, J. D., Rampey, R. A., & Zolman, B. K. (2014). Auxin input pathway disruptions are mitigated by changes in auxin biosynthetic gene expression in Arabidopsis. *Plant Physiology* 165(3), 1092-1104
- Stadtmueller, B. M., & Hill, C. P. (2011). Proteasome activators. *Mol Cell* 41(1), 8-19

- Staswick, P. E., Serban, B., Rowe, M., Tiryaki, I., Maldonado, M. T., Maldonado, M. C., & Suza, W. (2005). Characterization of an Arabidopsis enzyme family that conjugates amino acids to indole-3-acetic acid. *Plant Cell* 17(2), 616-627
- Strader, L. C., Monroe-Augustus, M., & Bartel, B. (2008). The IBR5 phosphatase promotes Arabidopsis auxin responses through a novel mechanism distinct from TIR1-mediated repressor degradation. *BMC Plant Biology* 8(41)
- Sun, S., Liu, S., Zhang, Z., Zeng, W., Sun, C., Tao, T., Lin, X., & Feng, X. H. (2017). Phosphatase UBLCP1 controls proteasome assembly. *Open Biology* 7(5), 170042
- Szemenyei, H., Hannon, M., & Long, J. A. (2008). TOPLESS mediates auxin-dependent transcriptional repression during Arabidopsis embryogenesis. *Science* 319(5868), 1384-1386
- Tan, X., Calderon-Villalobos, L. I. A., Sharon, M., Zheng, C., Robinson, C. V., Estelle, M., & Zheng, N. (2007). Mechanism of auxin perception by the TIR1 ubiquitin ligase. *Nature Articles* 446, 640-645
- Tiwari, S. B., Hagen, G., & Guilfoyle, T. J. (2004). Aux/IAA proteins contain a potent transcriptional repression domain. *The Plant Cell* 16(2), 533-543
- Tokumoto, M., Horiguchi, R., Nagahama, Y., & Tokumoto, T. (1999). Identification of the Xenopus 20S proteasome alpha4 subunit which is modified in the meiotic cell cycle. *Gene* 239(2), 301-308
- Tomko Jr., R. J., & Hochstrasser, M. (2013). Molecular architecture and assembly of the eukaryotic proteasome. *Annu Rev Biochem.* 2013, 82

- Uehara, T., Okushima, Y., Mimura, T., Tasaka, M., & Fukaki, H. (2008). Domain II mutations in CRANE/IAA18 suppress lateral root formation and affect shoot development in *Arabidopsis thaliana*. *Plant Cell Physiol.* 49(7), 1025-1038
- Ulmasov, T., Murfett, J., Hagen, G., & Guilfoyle, T. J. (1997). Aux/IAA proteins repress expression of reporter genes containing natural and highly active synthetic auxin response elements. *The Plant Cell* (9), 1963-1971
- Van der Krieken, W. M., Breteler, H., Visser, M. H. M., & Mavridou, D. (1993). The role of the conversion of IBA into IAA on root regeneration in apple: introduction of a test system. *Plant Cell Reports* 12(4), 203-206
- Vierstra, R. D. (2009). The ubiquitin-26S proteasome system at the nexus of plant biology. *Nature Reviews Molecular Cell Biology* 10, 385-397
- Villalobos, L. I. A. C., Lee, S., Oliveira, C. D., Ivetac, A., Brandt, W., Armitage, L., Sheard, L. B., Tan, X., Parry, G., Mao, H., Zheng, N., Napier, R., Kepinski, S., & Estelle, M. (2012). A combinatorial TIR1/AFB-Aux/IAA co-receptor system for differential sensing of auxin. *Nat Chem Biol.* 8(5), 477-485
- Wang, R., Zhang, Y., Kieffer, M., Yu, H., Kepinski, S., & Estelle, M. (2016). HSP90 regulates temperature-dependent seedling growth in *Arabidopsis* by stabilizing the auxin co-receptor F-box protein TIR1. *Nature Communications* 7(10269), doi: 10.1038/ncomms10269
- Wani, S. H., Kumar, V., Shriram, V., & Sah, S. K. (2016). Phytohormones and their metabolic engineering for abiotic stress tolerance in crop plants. *The Crop Journal* 4(3), 162-176

- Whitby, F. G., Masters, E. I., Kramer, L., Knowlton, J. R., Yao, Y., Wang, C. C., & Hill, C. P. (2000). Structural basis for the activation of 20S proteasomes by 11S regulators. *Nature* 408(6808), 115-120
- Willems, A. R., Schwab, M., & Tyers, M. (2004). A hitchhiker's guide to the cullin ubiquitin ligases: SCF and its kin. *Biochim Biophys Acta*. 1695(1-3), 133-170
- Winkler, M., Niermeyer, M., Hellmuth, A., Janitza, P., Christ, G., Samodelov, S. L., Wilde, V., Majovsky, P., Trujillo, M., Zurbriggen, M. D., Hoehenwarter, W., Quint, M., & Villalobos, L. I. A. C. (2017). Variation in auxin sensing guides AUX/IAA transcriptional repressor ubiquitylation and destruction. *Nat Commun*. 8, 15706
- Winter, D., Vinegar, B., Nahal, H., Ammar, R., Wilson, G. V., & Provart, N. J. (2007). An "electronic fluorescent pictograph" browser for exploring and analyzing large-scale biological data Sets. *PLoS ONE* 2(8), e718
- Yang, T., & Poovaiah, B. W. (2000). Molecular and biochemical evidence for the involvement of calcium/calmodulin in auxin action. *J Biol Chem*. 275(5), 3137-3143
- Yedidi, R. S., Wendler, P., & Enenkel, C. (2017). AAA-ATPases in Protein Degradation. *Front Mol Biosci*. 4(42), doi:10.3389/fmolb.2017.00042
- Yu, H., Zhang, Y., Moss, B. L., Bargmann, B. O. R., Wang, R., Prigge, M., Nemhauser, J., & Estelle, M. (2015). Untethering the TIR1 auxin receptor from the SCF complex increases its stability and inhibits auxin response. *Nat Plants*. 1(13), doi:10.1038/nplants.2014.30

- Zhang, W., Ito, H., Quint, M., Huang, H., Noel, L. D., & Gray, W. M. (2008). Genetic analysis of CAND1-CUL1 interactions in Arabidopsis supports a role for CAND1-mediated cycling of the SCF^{TIR1} complex. *PNAS* 105(24), 8470-8475
- Zolman, B. K., Yoder, A., & Bartel, B. (2000). Genetic analysis of indole-3-butyric acid responses in Arabidopsis thaliana reveals four mutant classes. *Genetics* 156(3), 1323-1337
- Zong, C., Gomes, A. V., Drews, O., Li, X., Young, G. W., Berhane, B., Qiao, X., French, S. W., Bardaq-Gorce, F., & Ping, P. (2006). Regulation of murine cardiac 20S proteasomes: role of associating partners. *Circ Res.* 99(4), 372-380
- Zulawski, M., Braginets, R., & Schulze, W. X. (2013). PhosPhAt goes kinases—searchable protein kinase target information in the plant phosphorylation site database PhosPhAt. *Nucleic Acids Research* 41, D1176-1184